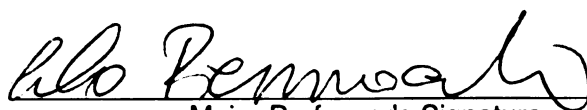This is to certify that the
dissertation entitled

MODEL OF AN EXCITON-PHOTON SYSTEM
INTERACTING WITH THE LATTICE

presented by

Mikhail Valeryevich Katkov

has been accepted towards fulfillment
of the requirements for the

_____Ph.D._____   degree in   _____Physics_____

_____
Major Professor's Signature

_____December 14, 2006_____

Date

PLACE IN RETURN BOX to remove this checkout from your record.
TO AVOID FINES return on or before date due.
MAY BE RECALLED with earlier due date if requested.

DATE DUE	DATE DUE	DATE DUE

2/05 p:/CIRC/DateDue.indd-p.1

MODEL OF AN EXCITON-PHOTON SYSTEM INTERACTING WITH THE LATTICE

By

Mikhail Valeryevich Katkov

A DISSERTATION

Submitted to
Michigan State University
in partial fulfillment of the requirements
for the degree of

DOCTOR OF PHILOSOPHY

Department of Physics and Astronomy

2006

ABSTRACT

MODEL OF AN EXCITON-PHOTON SYSTEM
INTERACTING WITH THE LATTICE

By

Mikhail Valeryevich Katkov

The purpose of my thesis is to provide a model and theoretical analysis of a matter-light system in which the exciton-phonon and the exciton-photon interactions are treated on the same ground. The system considered is a semiconductor polymer chain coupled to a single electromagnetic mode in a cavity. The excitations of the chain have a mixed exciton-photon character and are described as polaritons. Polaritons are coupled to the lattice by the deformation potential interaction and can propagate in the chain. I find that the presence of optical excitation in the polymer induces strain on the lattice. I use a BCS variational wave function to calculate the chemical potential of the polaritons as a function of their density. The validity of the variational approach is checked be analyzing the case of a short chain with only two unit cells. In the case of a long chain and for a strong coupling with the lattice, the system undergoes a phase transition corresponding to the self-trapping of polaritons. The role of the exciton spontaneous emission and cavity damping is discussed in the case of homogeneous optical lattice strain.

ACKNOWLEDGMENTS

I would like to thank my advisor Prof. Carlo Piermarocchi for his full support in both the professional and personal aspects.

Contents

List of Figures

List of Tables

Introduction

Recent advances in nanospectroscopy have demonstrated the possibility of addressing a single conjugated polymer chain in a solid matrix [1,2]. These optical studies of single chains overcome limitations due to ensemble averaging and inhomogeneous broadening and give a clear picture of the exciton dynamics. Most interestingly, a one-dimensional (1D) singularity in the optical density of states, a $T^{1/2}$ temperature dependence of the the exciton lifetime, [3] and a macroscopic quantum spatial coherence [4] have been observed in isolated red polydiacetylene (PDA) chains. These features suggest that the behavior of optical excitations in polymer chains can be very close to that of an ideal semiconductor quantum wire system.

In this thesis, we study excitons in a polymer chain coupled to a single electromagnetic mode in a cavity. The resulting mixed states of excitons and cavity photons can be described in terms of polariton quasiparticles. We will focus on the properties of polaritons in the presence of a deformation potential interaction with the lattice. The main contribution of this thesis consists in proposing and analyzing a new theoretical model which includes the essential physical ingredients in a simple and elegant manner. These essential ingredients are: the 1D nature of the optical excitations, the strong exciton-lattice coupling (polaronic effects) and the strong exciton-photon coupling (polaritonic effect). Polaronic and polaritonic effects in 1D systems have been separately studied in the past [5], [6], [7]. However, the interplay of these two strong interactions has not been studied before.

Excitons in polymer chains provide an example of a system where this interplay gives rise to new physical effects. The presence of an optical cavity enhances such effects because it enhances the light-matter coupling. We will consider a modified Su-Schrieffer-Heeger [8](SSH) model, describing the propagation of excitons in the polymer [7], with an additional term that takes into account the coupling with a single cavity mode. Excitons are modeled as excitation of two level systems localized within the unit cells of the polymer chain, and a variational mean-field approach is used to calculate the properties of the ground state of the systems at zero temperature as a function of the density of polaritons. A similar approach was used to study the transition between a polariton Bose Einstein condensate (BEC) to a laserlike behavior for polaritons in a cavity [9]. The coupling to the lattice by the deformation potential adds new features to the ground-state properties of polaritons. One of the main results of this thesis consists in showing that a self-trapping [10] of polaritons occurs at a threshold value for the polariton density. This means that even if the polymer chain is homogeneously excited, the polarization of the medium will be spatially inhomogeneous, showing bright spots coming from the luminescence of self-trapped polaritons. This mechanism could give rise to a BEC of polaritons which localize spontaneously without the need of external traps or strain fields.

Exciton-polaritons are one of the most promising candidates for the realization of BECs in condensed matter systems [11]. Exciton-polaritons lasing [12] and matter-based parametric amplifiers [13] are additional important applications of these quasiparticles. Exciton-polaritons in organic systems are particularly interesting due to the large excitonic oscillator strength and to their strong coupling to phonons, which gives rise to strong optical nonlinearities [14]. Evidence of polaritonic effects in a single polydiacetylene chains has been recently reported [15].

We will focus on semiconductor polymer chains with a non-degenerate ground state. In principle many different materials have the exciton-phonon coupling strong

enough for this optical self-trapping effect. [16] A well known example in this class of materials is polydiacetylene (PDA) [17], which we will use throughout the thesis. Polydiacetylene [18], has been studied for its strong nonresonant optical nonlinearities and exciton-phonon effects. Phonon-mediated optical nonlinearities have been observed in this material [14]. However, we will keep our theory general in such a way that it can be extended to polymers with similar properties.

The geometry of the system consists of a single polymer chain embedded in a 3D optical cavity. The total length of a polymer chain is typically of the same order or smaller than the wavelength of light at the exciton resonance. We consider only a single discrete cavity mode coupled to the excitons. This is justified by the fact that in organic systems the exciton bandwidth is of the order of several tens of meV, much smaller than the energy separation between the fundamental and first excited 0D cavity modes (typically around 2 eV). As a consequence the photon confinement, in contrast to other systems, the linear momentum is not a good quantum number for polaritons in this case. Different geometries for organic systems in optical cavity have been considered in the literature. For instance, an interesting interplay of the exciton-cavity and exciton-LO-phonon dynamics has been predicted in the case of planar cavity structures [19]. We chose the cavity fundamental mode energy below the exciton creation energy. Thus, there is no absorption of energy since the cavity photons are in the transparency region.

This thesis is organised as follows. First we give a review of the exciton concept in Chapter 1 as a composite particle of an electron and a hole held together by Coulomb attraction. We describe the two classes of excitons: *Frankel* and *Wannier*, giving commutation rules for the former and an effective hydrogenic model for the later, where we pay attention to the statistical properties of excitons.

In Chapter 2 we introduce the deformation potential, which is responsible for interaction of the excitons with acoustic phonons. Following Toyazawa [20], we show stability of a bound state due to exciton-phonon coupling in 1D. We

introduce the Su Schrieffer Heeger (SSH) Hamiltonian [6] which describes an exciton-lattice interacting system via the deformation potential. Using variational approach we show how to get a non-linear Schrödinger equation, describing the exciton localization. Then, we discuss an analytical solution to the equation in the case of an infinite polymer chain.

To obtain some parameters for a polymer chain such as the atomic positions, exciton mass, energy gap and deformation potential, we use *ab initio* quantum-mechanical calculations in Chapter 3. For these purposes we employ a set of programs for electronic structure calculations within the density functional theory (DFT). Also, we give a brief description of DFT in this Chapter. We find a good agreement of the results obtained from *ab initio* calculations with the experimental data.

In Chapter 4 we introduce the concept of polaritons as mixed states of photons and optical excitations. First we consider the problem of a two level system coupled to a single optical mode using the *dressed-atom* picture. Then we extend the model to a system of N two-level oscillators. After reviewing the concept of coherent states, we build a polariton wave function. To find the ground state we minimize the energy of the exciton-photon interacting system by the use of the variational approach. We analyze the chemical potential of the polariton system and a mixed exciton-photon nature of the system depending on the polariton density.

Our ultimate purpose is to combine these two types of interactions by considering an exciton-phonon system in a microcavity. In Chapter 5 we give our model of such a 1D system of excitons coupled to lattice deformations as well as to a single cavity mode of the electromagnetic field. The Hamiltonian of our model consists of two terms corresponding to the Dicke model [5] and the SSH model [21]. Also, we compare the variational results to an exact calculation with two sites in order to establish the validity of our approach. Since the system is strongly nonlinear, it is

hard to solve it analytically except for some limiting cases. We provide the details of the numerical energy minimization procedure (the steepest descent method of functional minimization) used to find the distribution of polaritons in the chain and the total energy of the systems.

The results on the self-trapping phase transition as well as analytical results that can be obtained is some limits are described in Chapter 6. We present there our results of the optical polarization function for different regimes of the self-trapping. The optical polarization localization induces local forces on the lattice, which create the lattice distortions. The chemical potential of the system and photon/exciton density shows a discontinuity at the points of the self-trapping phase transition because of the polariton number redistribution between the excitonic and photonic parts . Also, in the last part of this Chapter we analyze the role of the excitonic spontaneous emission and of the finite Q factor of the cavity. Conclusions are in the last Chapter, which also contains a discussion of possible experimental observations of the predicted effect.

Chapter 1

Excitons

In this chapter we will review the exciton concept, which will be used throughout this thesis. Simply put, an exciton is an electron and a hole held together by Coulomb attraction. An exciton localized within a single unit cell is called a *Frenkel* exciton. Frenkel excitons appear mainly in molecular crystals, polymers, and biological molecules. An exciton in the opposite limit is called a *Wannier* exciton, that corresponds to an electron hole pair spread over many unit cells. Wannier excitons are typical for inorganic semiconductors. In between these two limits, there are intermediate excitons. We will see that excitons in polydiacetylene (PDA) belong to this intermediate class and are therefore particularly difficult to describe theoretically.

In Section 1.1 we describe Frenkel excitons, and we introduce the paulion commutation rules for the exciton creation and annihilation operators. These Paulions commutator rules are a consequence of the composite nature of excitons. In Section 1.2 we introduce Wannier excitons, which are quite different from that of Frenkel excitons, and can be described using an effective hydrogenic model. Finally, in Section 1.3 we give a brief discussion of the exciton lifetime and the exciton statistical properties. In particular, we discuss the limitations of the bosonic approach.
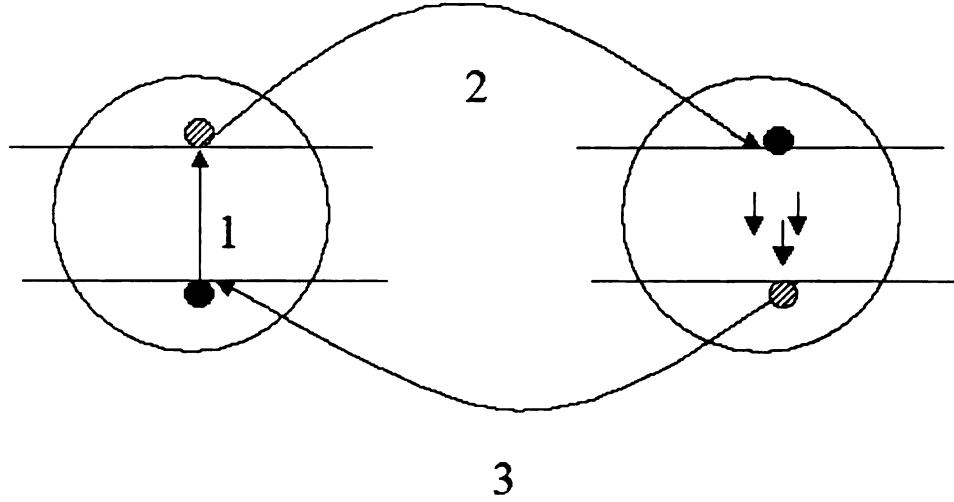
Figure 1.1: A physical picture of exciton hopping: 1) an electron is excited from a valence shell in the first unit cell; 2) it moves into unoccupied excited state of a nearby cell; 3) the Coulomb repulsion on the valence electrons in the second cell pushes a valence electron towards the hole left in the valence shell of the first cell.

1.1 Frenkel excitons

Excitons can move through a solid. In the case of Frenkel excitons, this motion is viewed as hopping of both the electron and the hole from one site to another. A physical picture of this looks as the following. An electron is excited from a valence shell. Then it may move into unoccupied excited state of a nearby cell. The Coulomb repulsion on the valence electrons in this excited cell pushes one valence electron towards the hole left in the valence shell of the original cell. This effectively makes the hole to follow the excited electron. The schematic of the process is shown in Fig. 1.1. Alternatively, it may be seen as an excited electron that attracts the hole in the valence shell of the new cell.

In general the Frenkel exciton Hamiltonian has the form [22]

$$H_{ex} = \sum_n E_g B_n^\dagger B_n + \sum_{nm} J_{n,m} B_n^\dagger B_m \, , \tag{1.1}$$

where $B_n^\dagger$, B_n are operators of creation and annihilation of an excitation at lattice

site n, respectively. E_g is the energy gap, and J_{nm} is the interaction parameter for a transfer between two molecules at site n and m. The first part of the Hamiltonian represents on-site excitation, while the second one describes the exciton transfer process.

The $B_n^\dagger$, B_n are Pauli operators [22], which obey Fermi anticommutation relations at the same site

$$B_n B_n^\dagger + B_n^\dagger B_n = 1 ,$$

$$B_n B_n = B_n^\dagger B_n^\dagger = 0 , \tag{1.2}$$

and Bose commutation relations between different sites

$$[B_n B_m^\dagger] = [B_n B_m] = [B_n^\dagger B_m^\dagger] = 0 , m \neq n , \tag{1.3}$$

The anticommutation relations forbid two excitons from being localized in the same unit sell. Applying a Fourier transformation to

$$B_n = \frac{1}{\sqrt{N}} \sum_k e^{-ikna} b_k , \tag{1.4}$$

where N is the number of lattice sites, k is the wave vector, a is the site separation in a periodical chain, we determine b_k as the annihilation operator of an exciton with a wave vector k. For b_k and $b_k^\dagger$ commutation relations are

$$[b_k, b_{k'}] = 0, \qquad [b_k^\dagger, b_{k'}^\dagger] = 0$$

and

$$[b_{k'}, b_k^\dagger] = \delta_{k,k'} - \frac{2 \sum_n B_n^\dagger B_n}{N} = \delta_{k,k'} - 2\frac{N_{ex}}{N} , \tag{1.5}$$

where N_{ex} is the number of excitons. Thus, at low-exciton concentration, the Pauli operator are replaced by Bose ones.

1.2 Wannier excitons

The picture of Wannier excitons is quite different [23]. In this picture, electrons and holes orbit each other as free particles in the background of the underlying lattice. The Wannier exciton can be seen as the analogous of a hydrogen atom. The underlying lattice is taken into account by the electron and hole mass renormalization, by the screening of the Coulomb interaction, and by considering the scattering with phonons and impurities.

The Wannier exciton wave function consists of an atomic-orbital part $\phi_n(x)$, which describes the relative electron-hole motion, and by a plane-wave factor $e^{i\mathbf{KR}}$ describing the electron-hole center of mass motion. In this phase term, $\mathbf{R}$ and $\mathbf{K}$ are the center of mass coordinate and wave vector, which corresponds to a crystal momentum. The total Wannier exciton energy is given by the expression:

$$E_{ex} = E_g + \frac{-e^2}{2a_{ex}\epsilon_0 n^2} + \frac{\hbar^2 K^2}{2(m_e + m_h)} , \tag{1.6}$$

where E_g is the electron-hole energy gap, a_{ex} is the excitonic Bohr radius,

$$a_{ex} = \frac{\hbar^2 \epsilon_0}{e^2 m_{ex}} , \tag{1.7}$$

m_{ex} is the reduced excitonic mass $m_{ex} = m_e m_h / (m_e + m_h)$. The energy spectrum is shown in Fig. 1.2. The Coulomb attraction is reduced by the static dielectric constant, ϵ_0. If the electron and hole masses are close to the free electron mass, the binding exciton energy is $\sim Ry/\epsilon_0^2$, where Ry is the Rydberg energy. For semiconductors, $\epsilon_0 \cong 10$, so the exciton binding energies are in the range of $100 meV$, and the separation between electron and hole is in the range of $50 Å$.
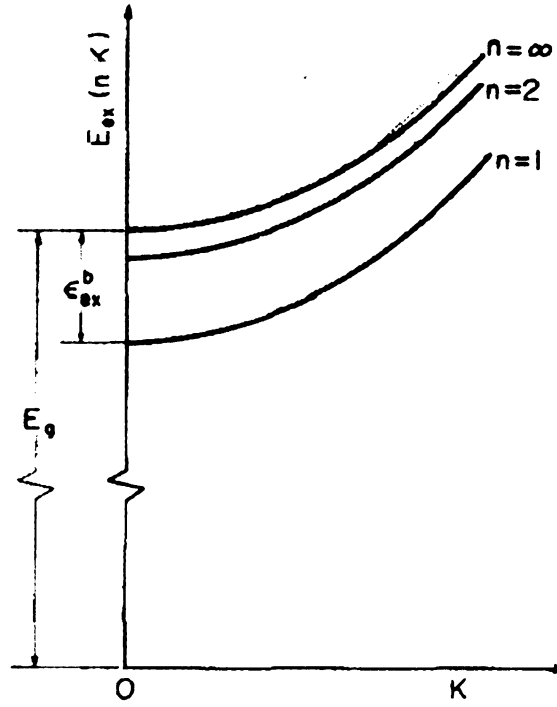
Figure 1.2: Pair excitation spectrum versus momentum K

1.3 Excitons as composite particles

Since excitons are made of particles and antiparticles, they intrinsically have a finite lifetime. Both Frenkel and Wannier excitons have a probability for the excited electron and the hole to recombine by photon emission. The recombination rate is proportional to the square of the electron-hole relative wave function at zero distance, which for a hydrogenic Wannier excitons is $\phi^2(0) = 1/\pi a_{ex}^3$. That implies that smaller excitons decay faster. In particular, Frenkel excitons are expected to have a shorter lifetime than Wannier excitons.

An exciton is composed of two fermions with spin $\frac{1}{2}$. So following the rules of angular momentum composition we have $\frac{1}{2} \otimes \frac{1}{2} = 0 \otimes 1$. This suggests that that excitons may behave as bosons. However, since they are composite bosons, this is

true only to a certain level of approximation. The classical review of Hanamura and Haug [24] derived the exciton commutation relationships in the general case, which we briefly present here.

The most general electron-hole pair state can be written in the form

$$|ex\rangle = \sum_{kk'} C_{kk'} a_k^\dagger b_{k'}^\dagger |0\rangle , \qquad (1.8)$$

where $a_k^\dagger$ and $b_k^\dagger$ are operators of electron and hole creation, and $|0\rangle$ is the vacuum state for pair generation.

If we determine the eigenfunctions of the Hamiltonian, which takes into account the crystal-band structure and includes the Coulomb interaction, and write $|ex\rangle = C_{K,n}^\dagger |0\rangle$, it can be obtained that

$$C_{K,n}^\dagger = \sum_{k,k'} \delta_{K,k+k'} \phi_n(l) a_k^\dagger b_{k'}^\dagger , \qquad (1.9)$$

with $l = (m_h/M)k - (m_e/M)k'$, where $M = m_e + m_h$, and $\phi_n(l) = \int d^3 \phi_n(x) e^{-il \cdot x}$ is the Fourier transform of the orbital wave function of the relative motion, which is the solution to the standard hydrogenic equation. The commutation relations of exciton operators are

$$[C_{K,n}, C_{K'n'}] = 0, \qquad [C_{K,n}^\dagger, C_{K'n'}^\dagger] = 0$$

and

$$
\begin{aligned}
[C_{K'n'}, C_{K,n}^\dagger] &= \delta_{K,K'} \delta_{n,n'} - \sum_l \phi_{n'}^*(\frac{m_h}{M}K' - l) \phi_n(\frac{m_h}{M}K - l) a_{K-l}^\dagger a_{K'-l} \\
&\quad - \sum_l \phi_{n'}^*(l - \frac{m_e}{M}K') \phi_n(l - \frac{m_e}{M}K) b_{K-l}^\dagger b_{K'-l} \\
&= \delta_{K,K'} \delta_{n,n'} + O(n a_{ex}^3) ,
\end{aligned} \qquad (1.10)
$$

11

where $n = N/V$ is the exciton density. We use the completeness of the orbital wave functions in the derivation. Thus, the excitons will act as bosons as long as the density of electronic excitation is small compared to a_{ex}^{-3}, or in other words the interparticle spacing is large compared with the correlation length a_{ex}.

Chapter 2

Exciton-lattice interaction

In this chapter we consider the interaction of electrons and excitons with the lattice in a one-dimensional system. We will see that this interaction results in a lattice deformation due to the coupling of the excitons or electrons with acoustic phonons via the deformation potential. In Section 2.1 we will first discuss the concept of deformation potential in a general way. Optical phonon modes are also present in polymer chains. However, we are not going to discuss their role since the optical excitation can be easily tuned far away from the vibronic resonances associated with the optical phonon modes. On the contrary, the acoustic phonons always present in the system, since there is no energy threshold for their creation. In Section 2.2 we discuss the simple heuristic version of Toyozawa's theory [20] showing that in 1D there is always a stable exciton bound state for a long chain due to the exciton-phonon coupling. In Section 2.3 we introduce the Su Schrieffer Heeger (SSH) Hamiltonian [6], which was developed to describe electron transport properties in polymer chains. Also in this chapter we derive a non-linear Schrödinger equation describing the exciton localization by deformation potential, and we discuss a simple analytical solution to that equation.

2.1 Deformation Potential

The concept of a linear deformation potential was first justified within the effective mass approximation by Bardeen and Shockley [25]. Within this theory, the energy of an electron in one band is expanded in powers of a quantity characterizing the strength of the lattice strain. The expansion is kept to the first power of this parameter, which makes the theory linear. Neglecting terms of the second order is equivalent to considering the effective masses unchanged by the strain.

Under applied forces a crystal is strained resulting in a change of volume and shape. The displacement of an ion in the crystal is characterized by

$$\mathbf{u} = \mathbf{r}' - \mathbf{r} \, , \tag{2.1}$$

where the position of the ion is $\mathbf{r}$ before the strain is applied and $\mathbf{r}'$ after it. When the crystal is strained, the distances between ions is affected. If the distance between two neighboring ions is initially

$$dl = \sqrt{dx_1^2 + dx_2^2 + dx_3^2} \, , \tag{2.2}$$

then after the strain is applied, it will be equal to

$$dl' = \sqrt{dx_1'^2 + dx_2'^2 + dx_3'^2}, \tag{2.3}$$

where $dx_i' = dx_i + du_i$. The distance dl'^2 can be expressed as

$$dl'^2 = dl^2 + 2\varepsilon_{ik}dx_i dx_k, \tag{2.4}$$

where a tensor of rank two has been introduced as

$$\varepsilon_{ik} = \frac{1}{2} \left(\frac{\partial u_i}{\partial x_k} + \frac{\partial u_k}{\partial x_i} + \frac{\partial u_l}{\partial x_i} \frac{\partial u_l}{\partial x_k} \right) . \tag{2.5}$$

14

The second rank tensor ε_{ik} is called the strain tensor. As it can be seen from the definition (2.5), this tensor is symmetric and can be therefore reduced by finding the three principal axes. Along the i-th principal axis the expression for the compressed length is

$$dx_i' = \sqrt{1 + 2\varepsilon_{ii}} dx_i .$$

(2.6)

In the case of a weak strain, we keep only the lowest order in the displacement. Then the components ε_{ik} of the strain tensor are determined by the expression

$$\varepsilon_{ik} = \frac{1}{2} \left(\frac{\partial u_i}{\partial x_k} + \frac{\partial u_k}{\partial x_i} \right) ,$$

(2.7)

and the relative elongation along the i-th axis is given by

$$\frac{dx_i' - dx_i}{dx_i} = \sqrt{1 + 2\varepsilon_{ii}} - 1 \approx \varepsilon_{ii} .$$

(2.8)

In general the energy shift for the k-th non-degenerate band extremum is expressed as

$$\Delta E^k = \sum_{ij} D_{ij} \varepsilon_{ij} .$$

(2.9)

The coefficients of this expansion form a second rank tensor called the deformation potential tensor. Note that ε_{ij} is a dimensionless quantity. In isotropic crystals, the deformation potential tensor is just a single coefficient, and

$$\sum_{ii} \varepsilon_{ii}(\mathbf{r}) = \text{div } \mathbf{u}(\mathbf{r})$$

(2.10)

represents a local elastic deformation in the continuum limit.

In this thesis we are going to consider semiconductor systems, and we will focus on the change in energy for the electronic states at the bottom of the conduction

band and at the top of valence band. These energy shifts are then written as

$$\Delta E_c = a_c \text{div } \mathbf{u(r)} \tag{2.11}$$

and

$$\Delta E_v = a_v \text{div } \mathbf{u(r)} \,, \tag{2.12}$$

where a_c and a_v are constants representing the deformation potentials for the conduction and valence band, respectively. The values of a_c and a_v can be obtained by measuring the carrier mobilities, or by a quantum-mechanical calculation of the band energy as a function of the lattice constant, which will be shown in Chapter 3. Deformation potentials are usually of the order of several electron volts [3] [7].

The displacement $u(\mathbf{r})$ can be expanded in terms of the acoustic modes of the lattice vibrations as

$$\mathbf{u(r)} = \sum_{\sigma\mathbf{q}} \sqrt{\frac{\hbar}{2\rho V S|\mathbf{q}|}} \mathbf{n}_{\sigma\mathbf{q}} (b_{\sigma\mathbf{q}} e^{i\mathbf{q}\mathbf{r}} + b_{\sigma\mathbf{q}}^\dagger e^{-i\mathbf{q}\mathbf{r}}) \,, \tag{2.13}$$

where ρ and S are the density and the longitudinal sound velocity in the crystal, $\mathbf{n}_{\sigma\mathbf{q}}$ is a unit vector in the direction of displacement of the normal mode, with $\sigma = 1, 2, 3$ representing the three branches of the acoustic mode, and V is the quantization volume. The relative compression of the volume is given by

$$\text{div } \mathbf{u(r)} = \sum_{\sigma\mathbf{q}} \sqrt{\frac{\hbar}{2\rho V S|\mathbf{q}|}} i\mathbf{q} \cdot \mathbf{n}_{\sigma\mathbf{q}} (b_{\sigma\mathbf{q}} e^{i\mathbf{q}\mathbf{r}} - b_{\sigma\mathbf{q}}^\dagger e^{-i\mathbf{q}\mathbf{r}}) \,. \tag{2.14}$$

This expression shows that only longitudinal phonon modes are involved in the deformation potential interaction in the linear approximation. Also, since the interaction coefficient in Eq. (2.14) is proportional to $q^{\frac{1}{2}}$, we notice that short-wavelength phonons play a dominant role.

In this thesis we will deal with excitons, composed by one electron and one hole. The deformation potential for an electron-hole pair is then written in the form

$$U(\mathbf{r}_e, \mathbf{r}_h) = a_e \text{div } \mathbf{u}(\mathbf{r}_e) - a_h \text{div } \mathbf{u}(\mathbf{r}_h) \ . \tag{2.15}$$

Thus, the exciton-phonon interaction results from the sum of phonon-electron and phonon-hole interaction. For a Frenkel exciton localized within a unit cell the expression (2.15) can be written as

$$U(\mathbf{r}_X) = a_X \text{div } \mathbf{u}(\mathbf{r}_X) \ , \tag{2.16}$$

where $a_X = a_e - a_h$ and $\mathbf{r}_x = \mathbf{r}_e = \mathbf{r}_h$.

2.2 Heuristic analysis

If the deformation potential interaction is strong enough, it may happen that the presence of an electron or an exciton causes a deformation of the lattice which in turn traps the carriers [26]. This self-trapping mechanism is referred to as a polaronic effect. In order to analyze the conditions for the self-trapping, we start by assuming that the electron is trapped in a region of length L. Thus, the electron kinetic energy due to the localization is $\hbar^2/2mL^2$, where m is either the exciton or electron mass. Also, we assume that the lattice is deformed locally , i e. only where the electron is. Assuming a constant expansion Δ in the length L, the elastic energy is $C\Delta^2 L/2$ (energy per length L, where C is an elastic constant). The electro-phonon interaction contributes to the total energy with an additional $-D\Delta$, where D is the deformation potential. Thus, the total energy is given in the form:

$$E = \frac{\hbar^2}{2mL^2} + \frac{C\Delta^2 L}{2} - D\Delta \ . \tag{2.17}$$

In order to understand the physical origin of the self trapping we first minimize the energy with respect to Δ, setting $\frac{\partial E}{\partial \Delta} = 0$. This leads to

$$\Delta = \frac{D}{CL} \cdot \qquad (2.18)$$

For this value of Δ the energy is

$$E = \frac{\hbar^2}{2mL^2} - \frac{D^2}{CL}, \qquad (2.19)$$

which has a minimum for any value of D at

$$L_{min} = \frac{\hbar^2}{mD^3} \cdot \qquad (2.20)$$

This shows that the minimum energy is

$$E_{min} = -\frac{D^4}{2C^2\hbar^2}, \qquad (2.21)$$

which implies that a stable bound state always exists in 1D case if the chain length is greater than the localization length L_{min}.

In the consideration above we used the adiabatic approximation assuming the excitons move faster than the lattice can respond. Since the vibrational energy quantum is much smaller than the exciton kinetic energy, the lattice motion can be treated classically. For the validity of using classical description in the adiabatic approximation

$$\frac{\hbar}{mS} >> L_{min}, \qquad (2.22)$$

where S is the sound velocity. $\hbar/mS$ is the analogy of the Compton wavelength, which is about 10^{-7} m for the typical semiconductor materials. Substituting the

expression (2.21) into the condition (2.22), we get

$$\frac{D^2}{\hbar SC} >> 1 \, , \tag{2.23}$$

which is satisfied for the most of semiconductive materials we consider.

2.3 SSH Hamiltonian

We will use the Su Schrieffer Heeger (SSH) Hamiltonian [6] to describe the interaction of excitons with the lattice displacement (phonons). The Hamiltonian describes the kinetic energy of the ions, the elastic energy of the lattice in the harmonic approximation, and the transfer energy which depends linearly on the relative displacement of the ions. It has the following form

$$H_{SSH} = \sum_n \frac{p_n^2}{2M} + \sum_n \frac{C}{2}(u_{n+1} - u_n)^2 - \sum_n t_{n+1,n}(B_{n+1}^\dagger B_n + B_n^\dagger B_{n+1}) \, . \tag{2.24}$$

M, C, u_n, and p_n are the mass, spring constant, total displacement, and momentum of the n-th site of the tight-binding chain. B_n^+, B_n are operators of creation, annihilation of excitons in a singlet spin state. The hopping term is $t_{n+1,n} = t_0 - \gamma(u_{n+1} - u_n)$, where γ is proportional to the exciton-phonon deformation potential interaction as $D = 2\gamma a$. If the lattice is given a uniform dilation d, then the exciton energy would increase by $2\gamma ad$. The value of t_0 can be determined by the exciton effective mass m as $t_0 = \hbar^2/2ma^2$.

In case of Frenkel excitons, they are localized within single unit cells. Thus the exciton wave-function can be written in the form

$$|\phi\rangle = \sum_n \beta_n B_n^\dagger |0\rangle_n \, , \tag{2.25}$$

where $|0\rangle_n$ means a state with no exciton at site n. Consider the adiabatic approxi-

mation defined by

$$\langle|H|\rangle = \langle\phi|H_{SSH}|\phi\rangle = H_L + H_{ex} , \tag{2.26}$$

which contains a free lattice and an excitonic term. The classical equations of motion for the chain in the adiabatic approximation [7] can be written as

$$M\ddot{u}_n = -\frac{\partial\langle H\rangle}{\partial u_n} = C(u_{n+1} - u_n) - C(u_n - u_{n-1}) + F_n . \tag{2.27}$$

In continuum limit, the strain force on the site n, F_n, is related to the gradient of the exciton density as

$$F_n = \frac{\gamma}{2}\frac{\partial|\beta_n|^2}{\partial n} . \tag{2.28}$$

For a stationary solution, we set Eq. (2.27) to zero, which gives the local displacement due to the strain force as

$$u_n = -C^{-1}\int\int F_n \, d^2n , \tag{2.29}$$

where n is a continuous variable now. Then from Eq. (2.28) we find

$$\frac{\partial u_n}{\partial n} = -\frac{\gamma}{2C}|\beta_n|^2 + a\Delta , \tag{2.30}$$

where Δ is a dimensionless constant of integration that gives finite-size effects. The choice of $\Delta = 0$ implies that the total length of the chain is not fixed, which does not affect the results in the limit of a wire much longer than the extension of the self-trapping region. The force constant C can be expressed in terms of the sound velocity S as $C = S^2 M/a^2$.

Using a variational approach, we can minimize the energy $\langle|H|\rangle$ (Eq. 2.26)with respect to the parameter β_n, which is subject to the constraint

$$\sum_n |\beta|^2 = 1 . \tag{2.31}$$

In continuum limit, that leads to the equation

$$-t_0(2\beta_n + \frac{\partial^2 \beta_n}{\partial n^2}) + \frac{D}{a}\beta_n\frac{\partial u_n}{\partial n} = \mu\beta_n \,,$$ (2.32)

where μ is a Lagrange multiplier. Then from Eqs. (2.30) and (2.32) we get the non-linear Schrödinger equation

$$-t_0(2\beta_n + \frac{\partial^2 \beta_n}{\partial n^2}) + \frac{D^2}{MS^2}\beta_n|\beta_n|^2 = \mu\beta_n \,.$$ (2.33)

The only solution describing the excitonic wave function to Eg. (2.33) which vanishes at infinity is

$$\beta = \sqrt{\frac{Y}{2}}\,\text{sech}[Y(n-n_0)] \,,$$ (2.34)

where

$$Y = \frac{D^2 m a^2}{2MS^2\hbar^2} \,,$$ (2.35)

Integrating Eq. 2.29, we get the lattice deformation as

$$u_n = -\frac{Da}{MS^2}\tanh[Y(n-n_0)] + na\Delta$$ (2.36)

For Δ equal to zero a chain must shorten on a polaron creation according to Eq. 2.36. In principle Δ can be choosen in such a way that the total length will be unchanged. The electronic energy is

$$E_{ex} = -2t_0 - \frac{mD^4 a^2}{8M^2 S^4 \hbar^2}$$ (2.37)

The first term is just the energy of a free exciton with $k = 0$ (an electron at the bottom of the conduction band and a hole at the top of the valence band). The second term is the exciton binding energy. The case of a finite chain, in which the localisation length is comparable to the chain length, is considered in Chapter 6.
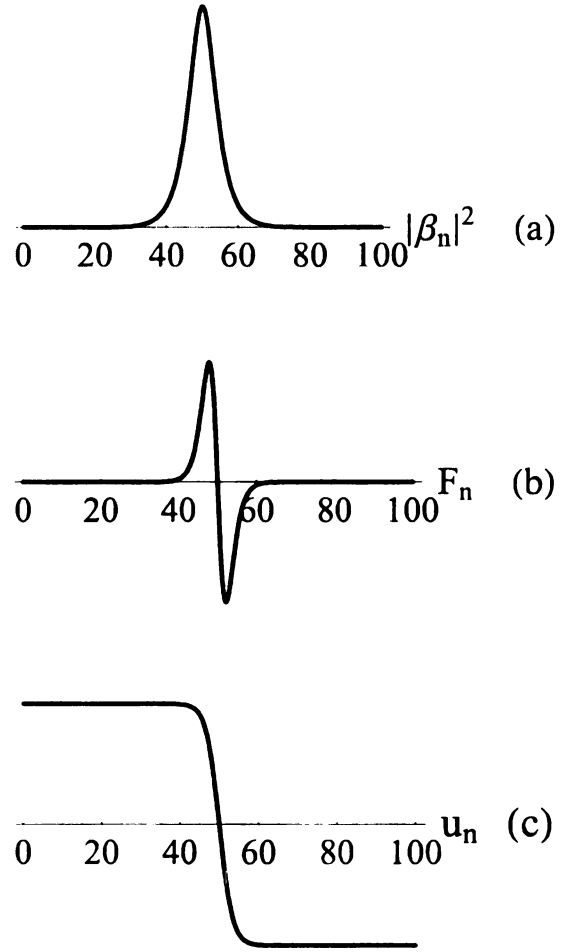
Figure 2.1: The dependence on the site index of (a) the exciton density, (b) the force due to the exciton density gradient, and (c) the displacement due to the force

Chapter 3

Ab initio electronic structure calculations

In order to obtain some parameters for our numerical calculations of the optical polarization function we used *ab initio* quantum-mechanical calculations. We have employed PWscf (Plane-Wave Self-Consistent Field), which is a set of programs for electronic structure calculations based on the density functional theory and density functional perturbation theory. This package uses plane wave basis sets and pseudopotentials. PWscf [27] can currently perform the following kinds of calculations:

- ground-state energy and one-electron (Kohn-Sham) orbitals

- atomic forces, stresses, and structural optimization

- molecular dynamics on the ground-state Born-Oppenheimer surface, also with variable-cell

- phonon frequencies and eigenvectors at a generic wave vector, using Density-Functional Perturbation Theory

- effective charges and dielectric tensors

- electron-phonon interaction coefficients for metals

- interatomic force constants in real space

In Section 3.1 we summarize the main results of the density functional theory (DFT), and in Section 3.2 we give a description of the methods used for the calculation. In Section 3.3 we present out numerical results for the band gap, electron/hole masses, and deformation potential for PDA (polydiacetylene). The results of these calculations are going to be used throughout the thesis as input parameters for our theoretical modeling.

3.1 Density Functional Theory

Traditional methods in electronic structure calculations are based on the many-electron wave function, for instance in the Hartree-Fock theory, which have a limited applicability because of the difficulties of the related formal equations. However, if the primary interest is in the ground-state properties rather than in the electronic excitations, there is an alternative and workable approach based on the density functional theory [30]. In this method the many-body electronic wave function is replaced by the electronic density as the basic quantity, and the calculation of ground-state properties is reduced exactly to a problem of noninteracting electrons in an effective potential. The effective potential includes the external potential and the effects of the Coulomb interactions between the electrons such as the exchange and correlation interactions. DFT is based on the Hohenberg-Kohn [28] variational principle, which relates the ground-state energy to the charge density. From this a set of one-electron-like self-consistent equations, the Kohn-Sham equations [29], can be derived, which give an exact description of ground-state properties at least in principle.

We will discuss below the derivation and some formalism of DFT. [29] As usual, we assume that the Born-Oppenheimer approximation is valid, meaning that elec-

trons move in an external potential V created by the nuclei of the considered molecules. An electron state is described by a wave function $\Psi(\vec{r}_1, \ldots, \vec{r}_N)$, which satisfies the many-electron Schrödinger equation

$$
H\Psi = [T + V + U]\,\Psi = \left[\sum_i^N -\frac{\hbar^2}{2m}\nabla_i^2 + \sum_i^N V(\vec{r}_i) + \sum_{i<j} U(\vec{r}_i, \vec{r}_j)\right]\Psi = E\Psi\,, \quad (3.1)
$$

where H is the electronic molecular Hamiltonian, N is the number of electrons and U is the electron-electron interaction. The operators T and U are so-called universal operators as they are the same for any system, while V is system dependent or non-universal. The difference between a single-particle problem and the much more complicated many-particle problem just arises from the interaction term U.

DFT provides a way to map the many-body problem with U onto a singe-body problem without U. In DFT the key variable is the density $n(\vec{r})$ given by

$$
n(\vec{r}) = N \int d^3r_2 \int d^3r_3 \cdots \int d^3r_N \Psi^*(\vec{r}, \vec{r}_2, \ldots, \vec{r}_N)\Psi(\vec{r}, \vec{r}_2, \ldots, \vec{r}_N)\,. \quad (3.2)
$$

Hohenberg and Kohn proved that this relation between the wave function and the density can be inverted for the ground state density $n_0(\vec{r})$, i.e. Ψ_0 is a unique functional of n_0,

$$
\Psi_0 = \Psi_0[n_0] \quad (3.3)
$$

Consequently, all other ground state observables F are also functionals of n_0

$$
\langle F \rangle [n_0] = \langle \Psi_0[n_0] | F | \Psi_0[n_0] \rangle\,. \quad (3.4)
$$

Thus the ground state energy is also a functional of n_0

$$
E_0 = E[n_0] = \langle \Psi_0[n_0] | T + V + U | \Psi_0[n_0] \rangle\,, \quad (3.5)
$$

where the external potential can be written explicitly in terms of the density

$$V[n] = \int V(\vec{r})n(\vec{r})\mathrm{d}^3r .$$ (3.6)

When V is known for a specific system the functional

$$E[n] = T[n] + U[n] + \int V(\vec{r})n(\vec{r})\mathrm{d}^3r$$ (3.7)

has to be minimized with respect to n, assuming reliable expressions for $T[n]$ and $U[n]$. The energy minimization will give the ground state density n_0 and all other ground state observables. By solving the so-called Kohn-Sham equations of the non-interacting system

$$\left[-\frac{\hbar^2}{2m}\nabla^2 + V_s(\vec{r}) \right] \phi_i(\vec{r}) = \epsilon_i\phi_i(\vec{r}) ,$$ (3.8)

we can find the orbitals ϕ_i that reproduce the density $n(\vec{r})$ of the original many-body system

$$n(\vec{r}) \equiv n_s(\vec{r}) = \sum_i^N |\phi_i(\vec{r})|^2 .$$ (3.9)

V_s is an external effective potential in which the particles are moving and it can be written as

$$V_s = V + \int \frac{e^2 n_s(\vec{r}')}{|\vec{r} - \vec{r}'|}\mathrm{d}^3r' + V_{\mathrm{XC}}[n_s(\vec{r})] ,$$ (3.10)

where the second term denotes the so-called Hartree term describing the electron-electron Coulomb repulsion, while the last term V_{XC} is called the exchange correlation potential, which includes all the many-particle interactions.

3.2 Calculation methods

The common procedure of all the DFT methods is based on solving the one-electron eigenvalue problem 3.8, where self-consistent iterations of the equation are required between the crystal potential and the electronic density [30]. The main difference in the different computational methods consists in the kind of functions used to expand the crystal eigenfunctions. On one hand the expansion in a plane-wave basis set appears naturally to describe electron wave functions of poorly localized electrons in the crystal, e.i conduction states as well as valence states close in energy to the Fermi level. On the other hand, an exceedingly high number of plane waves is needed to reproduce correctly the crystal core states. This difficulty can be overcome either by simulating the potential with a pseudo-potential which reproduces correctly the energies of the weakly bound states, or by orthogonalizing the plane waves to the core states. The first approach is referred to as the pseudopotential methods and the second one as the orthogonalized plane-wave methods (OPW). In order to review the essential aspects of the OPW methods, we consider the plane waves [30]

$$W_n(\mathbf{k}, \mathbf{r}) = \frac{1}{\sqrt{NV}} \exp[i(\mathbf{k} + \mathbf{h}_n) \cdot \mathbf{r}], \qquad (3.11)$$

where $\mathbf{k}$ is a vector in the Brillouin zone and $\mathbf{h}_n$ is a vector of the reciprocal lattice. Knowing the crystal core states $|\phi_c(\mathbf{k}, \mathbf{r})\rangle$, the projector $P^{core}(\mathbf{k})$ on the space spanned by them can be defined as

$$P^{core}(\mathbf{k}) = \sum_c |\phi_c(\mathbf{k}, \mathbf{r})\rangle\langle\phi_c(\mathbf{k}, \mathbf{r})| . \qquad (3.12)$$

Thus the orthogonalized plane wave $X_n(\mathbf{k}, \mathbf{r})$ can be defined by

$$X_n(\mathbf{k}, \mathbf{r}) = [1 - P^{core}(\mathbf{k})]W_n(\mathbf{k}, \mathbf{r}) . \qquad (3.13)$$

Using this basis, the secular equation no longer gives the core states, and the conduction and valence states can be reproduced by a small number of $X_n(\mathbf{k}, \mathbf{r})$. The crystal potential is represented by a sum of atomic-like potentials

$$V(\mathbf{r}) = \sum_{d\mu, \tau m} V(\mathbf{r} - \mathbf{d}_\mu - \tau_m) \, , \tag{3.14}$$

centered at the site $\mathbf{d}\mu$ of each elementary cell denoted by the lattice vector τm. Then the matrix elements can be expressed in terms of the Fourier transform of the atomic-like potentials as

$$V_\mu(\mathbf{q}) = \frac{1}{V} \int V(\mathbf{r}) \exp[i\mathbf{q} \cdot \mathbf{r} d\mathbf{r}] \, , \tag{3.15}$$

and the orthogonality terms are $\langle W_n(\mathbf{k} + \mathbf{h}_n, \mathbf{r}) | \phi_c(\mathbf{k}, \mathbf{r}) \rangle$. Thus the secular equation in this wave set reads

$$\langle X_n(\mathbf{k} + \mathbf{h}_n, \mathbf{r}) | H - E | X_n(\mathbf{k} + \mathbf{h}_n, \mathbf{r}) \rangle =$$
$$= [(\mathbf{k} + \mathbf{h}_m)^2 - E] \delta_{mn} + \sum_{d\mu} \exp[-i(\mathbf{h}_m - \mathbf{h}_n) \cdot \mathbf{d}_\mu] V_\mu(\mathbf{h}_m) - \mathbf{h}_n) +$$
$$+ \sum_c (E - E_c) \langle W_n(\mathbf{k}, \mathbf{r}) | \phi_c(\mathbf{k}, \mathbf{r}) \rangle | \langle \phi_c(\mathbf{k}, \mathbf{r}) | W_n(\mathbf{k}, \mathbf{r}) \rangle \, . \tag{3.16}$$

The basic idea of the pseudopotential method is, as mentioned above, to eliminate the core and try to reproduce its effect on the valence states by means of a fictitious potential. A pseudopotential can be generated in a variety of ways either through scattering theory, or by fitting atomic properties or crystal levels. Pseudopotentials arise naturally in the OPW methods, where Eq. 3.16 can be seen as a secular equation between plane waves with a nonlocal energy-dependent pseudopotential

$$V_{ps}(\mathbf{k} + \mathbf{h}_m, \mathbf{k} + \mathbf{h}_n, E) = \sum_{d\mu} \exp[-i(\mathbf{h}_m - \mathbf{h}_n) \cdot \mathbf{d}_\mu] V_\mu(\mathbf{h}_m) - \mathbf{h}_n) +$$
$$+ \sum_c (E - E_c) \langle W_n(\mathbf{k}, \mathbf{r}) | \phi_c(\mathbf{k}, \mathbf{r}) \rangle | \langle \phi_c(\mathbf{k}, \mathbf{r}) | W_n(\mathbf{k}, \mathbf{r}) \rangle \, . \tag{3.17}$$

The pseudopotential method can be seen as an OPW method without the core orthogonalization part, which adds a smooth function in the vicinity of the core. In a typical approach pseudopotentials are given in the form of few Fourier components [30]., thus the secular equation reads

$$\langle W_m(\mathbf{k}, \mathbf{r}, \mathbf{r}) | H - E | W_n(\mathbf{k}, \mathbf{r}, \mathbf{r}) \rangle =$$

$$= [(\mathbf{k} + \mathbf{h}_m)^2 - E] \delta_{mn} + \sum_{\mathbf{d}\mu} \exp[-i(\mathbf{h}_m - \mathbf{h}_n) \cdot \mathbf{d}_\mu] V_{ps,\mu}(\mathbf{h}_m - \mathbf{h}_n) . \quad (3.18)$$

In such approach the pseudopotential reproduces the effect of the total potential on the valence electrons.

3.3 Calculation results

In order to obtain some realistic parameters for the further numerical calculations of the structure properties, we have used PWscf to perform *ab initio* calculations on PDA. First we made a self-consistent calculations within the density functional theory for the atomic position and electron charge density. Performing molecular dynamics calculations on the ground-state with variable-cell, we determined the C, H atomic positions. The electron charge density is shown in Fig. 3.1, where darker regions correspond to a greater charge density. The corresponding structure of PDA is shown in Fig. 3.2. There are single bonds between $C_{1(2)}$ and $H_{1(2)}$ and also C_2 and C_3, double bonds between C_1 and C_2, and triple bonds between C_3 and C_4, which makes the distance between them shorter compared to that between the other C atoms. Then, we performed PDA band structure calculations. The bands calculated, using the plane wave basis sets, are shown in Fig. 3.3. Based on these result we obtained the following PDA parameters involved in the numerical calculation of the optical polarization function. The energy gap between the valence and conduction band measured at $k = 0$ is equal to $2.0eV$. The effective electron
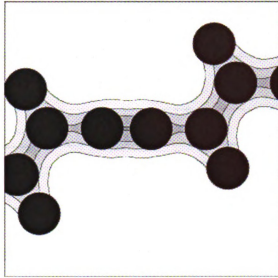
Figure 3.1: Polydiacetylene electron charge density distribution. Darker regions correspond to a greater charge density.
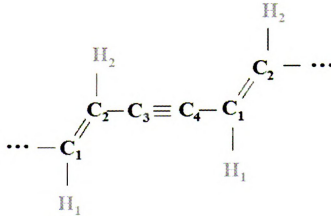
Figure 3.2: Structural model of a polydiacetylene chain with H atoms as side groups.

and hole masses calculated from the second derivatives of the dispersion curves of the conduct and valence bands at $k = 0$ are $0.25m_e$ and $0.36m_e$, correspondingly, where m_e is the electron mass. By changing a PDA unit cell length from the equilibrium, we get the PDA electron and hole deformation potentials: $D_e = 2.3eV$ and $D_h = -7.3eV$. The corresponding PDA exciton deformation potential determined as $D_e - D_h$ is $9.6eV$. Table 3.1 gives the calculated properties of PDA in comparison
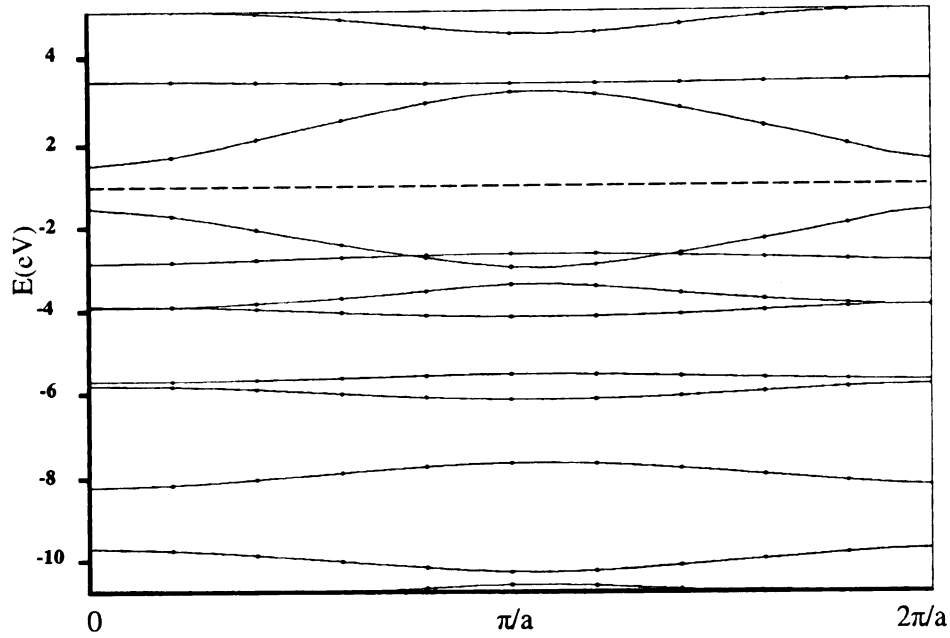
Figure 3.3: PDA band structure along the PDA symmetry axis in k-space. The dashed line is the zero level in the middle of the conductive and valence bands.

to those obtained from the experimental data [2], [7], [3].

	PWscf	experimental
E_g (eV)	2.0	2.3
$(m_e^* + m_h^*)/m_e$	0.6	0.3
$D_e - D_h$ (eV)	9.6	6.1

Table 3.1: *Ab initio* calculated PDA properties in comparison to the experimental data: energy gap; exciton mass; exciton deformation potential.

31

Chapter 4

Light-exciton interaction

In this chapter we will introduce the concept of polaritons as mixed states of photon and optical excitations. The simplest model for an optical excitation is given by a two-level oscillator, which will be considered here. The electromagnetic field will be described using a second quantization approach. This approach is important to describe many physical features as the spontaneous emission, the Lamb shift, resonance fluorescence, and "non-classical" states of light, such as squeezed states. In many problems, the state of the electromagnetic field can be described by coherent states. This approach is equivalent to a semiclassical description of the light-matter interaction. After reviewing the concept of coherent states, we will show how to build a polariton wave function using coherent states. This polariton wave function will be used in a variational approach throughout this thesis.

In Section 4.1 we review the second quantization for a single-mode electromagnetic field. In Section 4.2 we consider the problem of a two level system coupled to a single quantized mode, and we introduce the *dressed-atom* picture. In Section 4.3 we extend the model to N two-level oscillators coupled to a single cavity mode (the Dicke model). In Section 4.4 we define the *coherent* state of the electromagnetic field, which will be used to model a singe-mode electromagnetic field in an optical cavity. In Section 4.5 we introduce the variational wave function and find
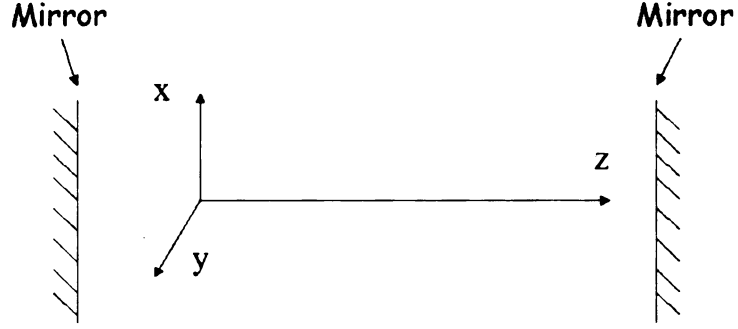
Figure 4.1: One dimensional cavity used to quantize electromagnetic field.

the ground state of the interacting excitons and photons.

4.1 Electromagnetic field quantization

We consider a cavity of volume V, enclosed by mirrors as shown in Fig. 4.1. Classically the electromagnetic field is described by the Hamiltonian

$$H = \int (\epsilon_0 E^2 + B^2/\mu_0) dV , \qquad (4.1)$$

where E and B are the magnitudes of the electric and magnetic fields, ϵ_0 and μ_0 are the permittivity constants, respectively. The integral is taken over the volume V. In the second quantization form, the Hamiltonian for the field can be rewritten in terms of the photon annihilation and creation operators c and $c^\dagger$ as

$$H = \hbar\omega_c(c^\dagger c + 1/2) . \qquad (4.2)$$

The corresponding eigenstates of the Hamiltonian satisfy the equation

$$H|n\rangle = \hbar\omega_c(n + 1/2) , \qquad (4.3)$$

where n may be interpreted as the *number of photons* in the state $|n\rangle$. The electric field operator can be expressed in terms of creation and annihilation operators as

$$E = \mathcal{E}(c + c^\dagger) \,, \tag{4.4}$$

where the *electric field per photon* is given by

$$\mathcal{E} = \sqrt{\frac{\hbar\omega_c}{\epsilon_0 V}} \,, \tag{4.5}$$

and the action of creation, annihilation operators on $|n\rangle$ is

$$
\begin{aligned}
c|n\rangle &= \sqrt{n}|n - 1\rangle \\
c^\dagger|n\rangle &= \sqrt{n+1}|n + 1\rangle \,,
\end{aligned} \tag{4.6}
$$

respectively.

4.2 Two level system coupled to a single cavity mode: dressed states

In describing the matter-field interaction we start with the simple problem of a two-level atom coupled to a single quantized mode of the field, and we introduce the so-called "dressed-atom" picture. [31]. The interaction Hamiltonian between an atom and the electric field in the dipole approximation has the form

$$V = -\mathbf{d} \cdot \mathbf{E} \,, \tag{4.7}$$

where $\mathbf{E}$ is the electric field and $\mathbf{d}$ is the dipole moment. For quantized fields, $\mathbf{E}$ and $\mathbf{d}$ become the dipole moment and electric field operators, respectively. Using

photon operators, the interaction Hamiltonian becomes

$$V = \frac{1}{2}(c + c^\dagger)(gB^\dagger + g^*B) \,, \tag{4.8}$$

where $B^\dagger$ and B are operators of creation and annihilation of an optical excitation. The full Hamiltonian for the two level system and the electromagnetic field then reads

$$H_{AL} = \hbar\omega_c c^\dagger c + \frac{1}{2}(c + c^\dagger)(gB^\dagger + g^*B) + E_g B^\dagger B \,, \tag{4.9}$$

where E_g is the energy difference between the ground and the first excited states. The coupling constant g can be chosen to be real without loss of generality.

A basic concept we will use in this thesis is the rotating-frame approximation. Considering the terms in the interaction energy Eq.(4.9), we note that $cB^\dagger$ corresponds to the absorbtion of a photon and the excitation of the atom. Conversely, $c^\dagger B$ corresponds to the emission of a photon and the deexcitation of the atom. These two combinations are kept in the rotating-frame approximation, and the remaining two pairs, $c^\dagger B^\dagger$ and cB, are dropped in this approximation. This can be clarified by writing the time evolution of the operators in the Heisenberg picture as

$$
\begin{aligned}
c(t)B^\dagger(t) &= c(0)B^\dagger(0)e^{-i(\hbar\omega c - Eg)t} \\
c(t)^\dagger B(t) &= c(0)^\dagger B(0)e^{i(\hbar\omega c - Eg)t} \,.
\end{aligned}
\tag{4.10}
$$

Notice that these "resonant" pairs vary very slowly when the energies of the photon and the excitation are close. On the contrary, the antiresonant terms

$$
\begin{aligned}
c(t)B(t) &= c(0)B(0)e^{-i(\hbar\omega c + Eg)t} \\
c(t)^\dagger B(t)^\dagger &= c(0)^\dagger B(0)^\dagger e^{i(\hbar\omega c + Eg)t} \,,
\end{aligned}
\tag{4.11}
$$

oscillates very fast and tend to average to zero. Dropping the combinations (4.11), we obtain the Hamiltonian

$$H_{AL} = \hbar\omega_c c^\dagger c + E_g B^\dagger B + \frac{1}{2}g(cB^\dagger + c^\dagger B) \, . \tag{4.12}$$

Notice that the light matter interaction couples only the atom-field states $|n,1\rangle$ and $|n+1,0\rangle$ for each value of n. We can break then the Hilbert space of the cavity photon system in many decoupled manifolds and we consider each manifold independently. Solving the secular equation on a given manifold, we get the energy eigenvalues

$$
\begin{aligned}
E_l &= E_g + n\hbar\omega_c - \frac{1}{2}(\mathcal{R}_n + \delta) \\
E_h &= \hbar(n+1)\hbar\omega_c + \frac{1}{2}(\mathcal{R}_n + \delta) \, ,
\end{aligned}
\tag{4.13}
$$

where the detuning

$$\delta = E_g - \hbar\omega_c \tag{4.14}$$

and the quantized Rabi frequency

$$\mathcal{R}_n = \sqrt{\delta^2 + g^2(n+1)} \, . \tag{4.15}$$

The energy eigenvectors are

$$
\begin{aligned}
|l\rangle &= \cos\theta_n|n,1\rangle - \sin\theta_n|n+1,0\rangle \\
|h\rangle &= \sin\theta_n|n,1\rangle + \cos\theta_n|n+1,0\rangle \, ,
\end{aligned}
\tag{4.16}
$$

36

where

$$\cos \theta_n = \frac{\mathcal{R}_n - \delta}{\sqrt{(\mathcal{R}_n - \delta)^2 + g^2(n+1)}},$$

$$\sin \theta_n = \frac{g\sqrt{n+1}}{\sqrt{(\mathcal{R}_n - \delta)^2 + g^2(n+1)}}. \qquad (4.17)$$

The state given by Eq. (4.16) are called dressed states describing the two-level atom interacting with a single-mode field in a given fixed number state for the photon field. The unperturbed states of noninteracting Hamiltonian are called bare states.

The energy separation between two dressed states within the same manifold is $\mathcal{R}_n$, which reaches its minimum at resonance when $E_g = \omega_c$. In this case, the dressed states Eq. (4.16) reduce to

$$|l\rangle = \frac{1}{\sqrt{2}}(|n,1\rangle - |n+1,0\rangle)$$

$$|h\rangle = \frac{1}{\sqrt{2}}(|n,1\rangle + |n+1,0\rangle) \qquad (4.18)$$

with eigenvalues

$$E_l = \hbar(n+1)\omega_c - \frac{1}{2}\hbar g\sqrt{n+1}$$

$$E_h = \hbar(n+1)\omega_c + \frac{1}{2}\hbar g\sqrt{n+1}. \qquad (4.19)$$

Dressed atom energy level diagram is shown in Fig. 4.2. We note that the rotating frame approximation will hold as long as $|\delta|$ remains much smaller than ω_c and E_g.
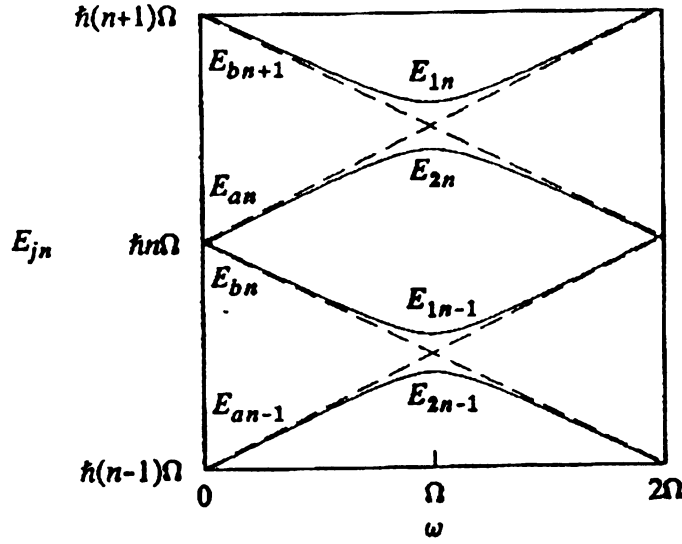
Figure 4.2: *Elements of quantum optics / Pierre Meystre, Murray Sargent III. Berlin; New York: Springer-Verlag, 1990.* Dressed atom energy level diagram. The dashed lines are energy iegenvalues for atom-field system with no interaction energy. Solid lines include atom-field interaction.

4.3 N two level systems coupled to a cavity mode: Dicke model

In order to introduce the polariton concept which we will use later for a chain, we consider the Dicke model [5] which describes localized, physically separated, saturable excitations coupled to a single mode of the electromagnetic field by the dipole interaction. We extend the Hamiltonian for a single two level system in Eq. (4.9) to a set of N two-level atoms. In the rotation-wave approximation discussed above, the Hamiltonian has the form

$$H_D = \hbar\omega_c c^\dagger c + \sum_n \frac{g}{2}(B_n^\dagger c + c^\dagger B_n) + \sum_n E_g B_n^\dagger B_n . \tag{4.20}$$

If the two-level atoms are near the ground states $\sum_n \langle B_n^\dagger B_n \rangle \ll N$, the operator

$$S^\dagger = \frac{1}{\sqrt{N}} \sum_n B_n^\dagger, \tag{4.21}$$

which creates the photon-exciton coupling, is approximately bosonic, and the Hamiltonian (4.20) is that of two coupled bosons. (Here we rescale the coupling constant $g' = g\sqrt{N}$) Polaritons are defined as eigenstates of such a model. To extend the polariton concept beyond the low-excitation limit, following Estham and Littlewood [32], we generalize the concept of a polariton by defining it as a quantum of excitation of the coupled light-matter system. The polariton number is then the total number of photons and excitons,

$$N_P = \langle c^\dagger c + \sum_n B_n^\dagger B_n \rangle, \tag{4.22}$$

which is a conserved quantity for the model.

4.4 Coherent states

We will describe the state of the field in the cavity in terms of coherent states, rather than with photon number states. In fact, it can be proved that the electromagnetic field in an optical cavity can be well represented by a coherent state [33]. A coherent state distributes its quantum-mechanical uncertainty equally, which means that the phase and amplitude uncertainty are approximately equal. Conversely, in a Fock state with a well-defined number of particles the phase is completely uncertain.

There are several ways to introduce coherent states. To emphasize their nearly classical character, we define the coherent states by the constraint that the classical energy of the field is equal to the quantum-mechanical energy for a coherent state

$|\zeta\rangle$. That leads to the factorization condition

$$\langle \zeta | c^\dagger c | \zeta \rangle = \langle \zeta | c^\dagger | \zeta \rangle \langle \zeta | c | \zeta \rangle \; . \tag{4.23}$$

It can be shown that the definition (4.23) implies that the coherent states are eigenstates of the annihilation operator

$$c | \zeta \rangle_\lambda = \lambda | \zeta \rangle_\lambda \; , \tag{4.24}$$

which can be used as an equivalent definition of the coherent states. The coherent state $|\zeta\rangle$ can be expressed in terms of the number states $|n\rangle$ as

$$|\zeta\rangle_\lambda = e^{-|\lambda|^2/2} \sum_n \frac{\lambda^n}{\sqrt{n!}} |n\rangle \; . \tag{4.25}$$

This gives the probability of finding n photons in the coherent state as

$$P(n) = e^{-\langle n \rangle} \frac{\langle n \rangle^n}{n!} \; , \tag{4.26}$$

which is called a Poisson distribution, where $\langle n \rangle$ is the average photon number. For a coherent state we have $\langle n \rangle = |\lambda|^2$.

A coherent state can also be expressed in terms of the vacuum state $|0\rangle$ as

$$|\zeta\rangle_\lambda = e^{\lambda c^\dagger - \lambda^* c} |0\rangle = D(\lambda) |0\rangle \; , \tag{4.27}$$

where $D(\geq)$ is called the displacement operator. The displacement operator can be seen as a shifting operator for the vacuum, and the coherent states $|\zeta\rangle$ are often called *displaced states of the vacuum*.

4.5 Variational Polariton wave function and energy minimization

We choose a trial wave function for the system of two level atoms as a superposition of a coherent state of photons and a BCS state of the fermions [32] in the form

$$|\lambda, \alpha, \beta, \varphi\rangle = |\zeta\rangle_\lambda \prod_n \left(\alpha_n |0\rangle_n + e^{i\varphi_n} \beta_n |1\rangle_n\right), \tag{4.28}$$

where $|\zeta\rangle_\lambda$ is the coherent state of the cavity mode with the order parameter λ, and $|0\rangle_n$ and $|1\rangle_n$ denote the number of excitons in the site n. λ, α_n, β_n, and φ_n are variational parameters, α_n and β_n are subject to the single-occupancy constraint

$$|\alpha_n|^2 + |\beta_n|^2 = 1. \tag{4.29}$$

We fix the overall phase in such a way to have λ real and introduce the phase φ_n to make α_n and β_n real.

By introducing the optical polarization function

$$\psi_n = -\langle B_n^\dagger + B_n\rangle = 2\alpha_n\beta_n, \tag{4.30}$$

the total energy reads

$$E = \hbar\omega_c\lambda^2 + \frac{g\lambda}{2}\sum_n \psi_n \cos\varphi_n dn - \frac{E_g}{2}\sum_n \sqrt{1 - \psi_n^2}, \tag{4.31}$$

in the assumption $|\alpha_n| > |\beta_n|$.

To find the ground state of the system at a fixed $\langle N_P\rangle$ we minimize the functional $\langle H - \mu N_P\rangle$ with respect to the function ψ_n and with respect to the λ and φ_n parameters. By minimizing the energy with respect to φ, we can set $\varphi_n = \pi$ assuming $g > 0$ and $\alpha_n\beta_n > 0$. Finally, the excitation parameters ψ_n and λ are given

by the solutions of

$$-g\lambda + (E_g - \mu)\frac{\psi_n}{\sqrt{1 - \psi_n^2}} = 0 \, , \tag{4.32}$$

$$(\hbar\omega_c - \mu)\lambda - \frac{g}{4}\sum_n \psi_n = 0 \, , \tag{4.33}$$

where μ is a Lagrange multiplier constraining the average polariton number, which plays a role of the chemical potential of the polariton system. Since the system is composed of N identical and noninteracting two level atoms, the variational coefficients, and therefore the polarization function ψ_n do not depend on the index n. We will see later in this thesis that the interaction with the lattice will break this symmetry.

After rescaling $\lambda' = \lambda/\sqrt{N}$ and $g' = g\sqrt{N}$ and eliminating ψ_n in Eqs. (4.32) and (4.33), we get the equation for the chemical potential

$$\tilde{\omega}_c = \frac{1}{4}\frac{g'^2}{\sqrt{\tilde{E}_g^2 + g'^2\lambda'^2}} \, , \tag{4.34}$$

where $\hbar\tilde{\omega}_c = \hbar\omega_c - \mu$ and $\hbar\tilde{E}_g = \hbar E_g - \mu$. Equation (4.34) is analogous to BCS gap equation, with an order parameter λ'.

At a very low polariton density μ can be obtained by expanding the Eq. (4.34) for small λ as

$$\mu = \frac{1}{2}(E_g + \hbar\omega_c - \sqrt{\delta^2 + g'^2}) \, , \tag{4.35}$$

where $\delta = E_g - \hbar\omega_c$ is the optical detuning. Notice that in this low density limit the chemical potential corresponds to the energy of the lowest dressed cavity-exciton state, i.e. the lower polariton. At finite polariton number we can calculate μ numerically. The results of our numerical calculations for the μ dependence on the polariton density $\rho_p = N_p/N$ are given in Fig. 4.3 for several values of the detuning δ. At low densities the μ is given by the conventional linear-response polariton energy (4.35). When the density increases the excitonic component of the polariton pop-
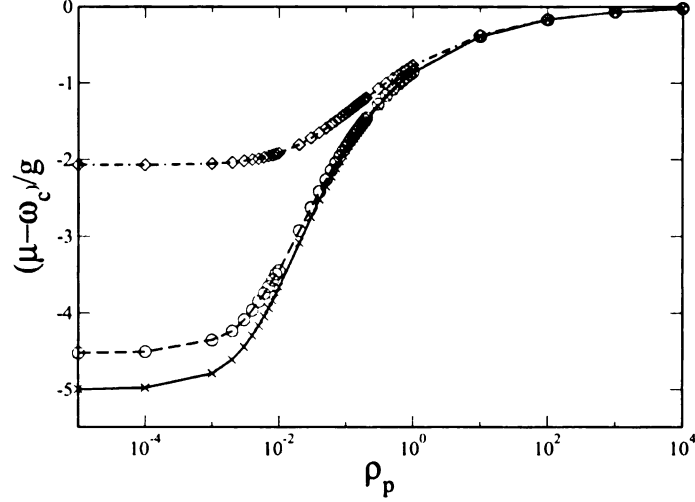
Figure 4.3: Polariton chemical potential as a function of the polariton density for $\delta/g = 0$ solid line, $\delta/g = 1$ (dashed line), and $\delta/g = 10$ ((dot-dashed line). At low density μ corresponds to the lower polariton energy, at large density the chemical potential become equal to the energy of the cavity photon since the excitonic component is saturated.

ulation saturates, and the polaritons become more photon-like. As a consequence we obtain that at high densities the chemical potential approaches $\hbar\omega_c$, which is the energy of the cavity photon.

Fig. 4.4 shows the exciton density $(\int |\beta_n|^2 dn)/N$ times 2 for the same parameters as in Fig. 4.3 as a function of ρ_p. Notice that this quantity reaches 1 in the limit of large polariton density, corresponding to a half filling of the excited electronic states. This maximizes the polarization and hence minimizes the dipolar interaction energy between the excitons and the cavity.

43
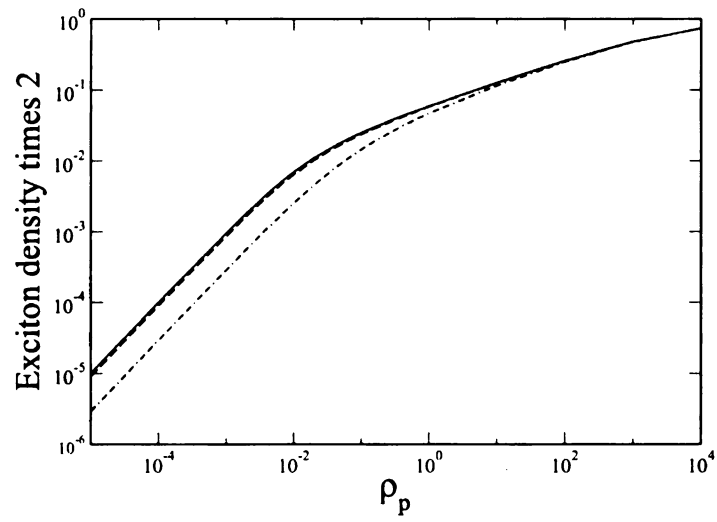
Figure 4.4: Exciton density times 2 as a function of excitation density for $\delta/g = 0$ (solid line), $\delta/g = 1$ (dashed line), and $\delta/g = 10$ (dot-dashed line). In the limit of a large polariton pooulation the exciton density saturates at half filling.

Chapter 5

Exciton-phonon interaction in a microcavity

In Chapter 2 we studied the interaction of excitons with the lattice (phonons) in a one-dimensional system. In that case, the exciton-photon interaction just represented a pumping mechanism to generate the exciton population. On the other hand, in Chapter 4 we describe the model of N two-level oscillators coupled to a single cavity mode. Of course, it would be of interest to treat the exciton-phonon and the exciton-photon interactions on the same ground. By considering the two interactions coherently, we can expect the possibility of controlling the system by some field parameters such as the polariton number and the cavity-exciton detuning. This Chapter deals with the exciton-photon and exciton-phonon models and is organized as follows: in Sect. 5.1 we introduce the model. In Sec. 5.2 we illustrate the variational approach used to calculate the ground state properties of the system. In Sec. 5.3 we compare the variational results to an exact calculation with two sites in order to establish the validity of our approach. In this Chapter the model and its limitations are discussed. The main results will be presented in Chapter 6.

5.1 The model

The model consists of the 1D system of excitons coupled to lattice deformations as well as to a single cavity mode of the electromagnetic field. The Hamiltonian can be written as

$$H = H_D + H_{SSH} \, . \tag{5.1}$$

The first term corresponds to the Dicke model [5] of an ensemble of two level systems coupled to a single electromagnetic mode

$$H_D = \omega_c c^\dagger c + \sum_n \frac{g}{2} (B_n^\dagger c + c^\dagger B_n) + \omega_X \sum_n B_n^\dagger B_n \, , \tag{5.2}$$

where ω_X is the exciton energy. We will use $\hbar = 1$ throughout the Chapter. $B_n^\dagger$ and B_n are operators of creation and annihilation of excitons in a singlet spin state, and $c^\dagger$ and c are creation and annihilation operators for the cavity photons of energy ω_c. Each site n of the model represents a single monomer of the polymer chain. The parameter g indicates the exciton-cavity dipolar coupling constant. In the Dicke model, the atoms do not have translational degrees of freedom and there is no direct transfer of optical excitation from one atom to the other. Here, we need to add two additional features to the Dicke model: (*i*) the excitations can hop from site to site and move along the backbone of the polymer chain, and, (*ii*), the hopping of the excitation depends on the relative position of the sites in the lattice, which can move around their equilibrium position. As discussed in Chapter 2, this can be represented by the excitation transfer in the SSH form as

$$
\begin{aligned}
H_{SSH} = & \sum_n \frac{p_n^2}{2M} + \sum_n \frac{C}{2} (u_{n+1} - u_n)^2 \\
& - \sum_n t_{n+1,n} (B_{n+1}^\dagger B_n + B_n^\dagger B_{n+1}) \, ,
\end{aligned}
\tag{5.3}
$$

where $t_{n+1,n} = t_0 - \gamma(u_{n+1} - u_n)$. The SSH model was used to describe the electronic transport in polyacetylene chains [8], and was extended to the case of excitonic transport in polydiacetylene [7]. We use the same definitions for the parameters as in Chapter 2.

We consider a 3D optical cavity giving a discrete spectrum of cavity modes. The size of the cavity can be chosen so that the fundamental mode at energy ω_c is resonant or nearly resonant with the exciton energy. Typically, the total length of the polymer chain is smaller than the wavelength of the light, therefore we can assume that the strength of the light-matter interaction g is constant in the site index n. Also, in the case of organic materials the excitonic bandwidth, given by $2t_0$, is of the order of several tens of meV, while the energy separation between different 3D cavity modes is typically around 2 eV. Therefore, the coupling of excitons with higher cavity modes can be neglected.

5.2   Energy minimization

We consider a polariton trial wave function which is a product of a coherent state for photons and a BCS state for excitons as [32]

$$|\lambda, \alpha, \beta, \varphi\rangle = |\lambda\rangle \prod_n \left(\alpha_n |0\rangle_n + e^{i\varphi n} \beta_n |1\rangle_n \right) , \qquad (5.4)$$

where λ, α_n, β_n, and φ_n are variational parameters, and $|\lambda\rangle$ represents a coherent state for the cavity. The coefficients α_n and β_n are subject to the single-occupancy constraint

$$|\alpha_n|^2 + |\beta_n|^2 = 1 . \qquad (5.5)$$

$|0\rangle$ is the vacuum state of the cavity mode, and $|0\rangle_n$ and $|1\rangle_n$ denote the ground and the excited state of the two level system at the site n. We assume λ real and we fix the overall phase to make α_n and β_n real. In contract to the discussion in Chapter

4, due to the hopping, the variational coefficients will depend on the index n in the general case.

We can interpolate continuously the wave function by transforming the discrete sum $\sum_{n=1}^{N}$ in a continuous integral $\int_{0}^{N} dv$. In this way, we can define the optical polarization $\psi(v) = 2\alpha(v)\beta(v)$, where α and β are continuous functions of v. We can express the total energy of the system as the expectation value of the Hamiltonian in Eq. (5.1) with the trial wave function in Eq. (5.4). In continuum form, the total energy can be expressed as

$$E = \omega_c \lambda^2 \tag{5.6}$$

$$+ \frac{1}{2} \int_{0}^{N} \left[\frac{p^2}{M} + Cu'^2 + t_0(\psi'^2 + \psi^2\varphi'^2) - t_0\psi^2 + \gamma u'\psi^2 + g\lambda\psi\cos\varphi - \omega_X\sqrt{1 - \psi^2} \right] dv,$$

where $\varphi(v)$, $p(v)$ and $u(v)$ are also continuous functions. The prime indicates the derivative with respect to the variable v. In deriving Eq. (5.6) we have assumed that $|\alpha(v)| > |\beta(v)|$ along the chain, which corresponds to the condition of negative detuning between the exciton resonance and the cavity mode. Notice that the total polariton number

$$N_P = \lambda^2 + \int |\beta|^2 dv = \lambda^2 + \frac{N}{2} - \frac{1}{2} \int \sqrt{1 - \psi^2} dv \tag{5.7}$$

is a conserved quantity. In order to find the ground state of the system at a fixed polariton number we perform a variational minimization of $\langle H - \mu N_P \rangle$ with respect to the functions ψ, φ, u and with respect to the constant λ. From the condition

$\delta(E - \mu N_P) = 0$ we obtain the system of equations

$$t_0(\varphi''\psi^2 + \varphi'\psi^{2'}) + \frac{g\lambda}{2}\psi\sin\varphi = 0 , \qquad (5.8a)$$

$$Cu'' + \frac{\gamma}{2}\psi^{2'} = 0 , \qquad (5.8b)$$

$$2t_0\psi'' + 2t_0\psi(1 - \varphi'^2) - 2\gamma\psi u' - g\lambda\cos\varphi - \frac{(\omega_X - \mu)\psi}{\sqrt{1 - \psi^2}} = 0 , \qquad (5.8c)$$

$$(\omega_c - \mu)\lambda + \frac{g}{4}\int \psi\cos\varphi dv = 0 . \qquad (5.8d)$$

From Eqs. (5.8a) and (5.6) we can see immediately that, in the assumption $\alpha\beta > 0$, and $g > 0$ we can take the solution $\varphi = \pi$, since this variable has no constraint. That makes the global phase of the optical polarization constant along the chain and out of phase with respect to the cavity field. In order to have a closed equation for ψ we can integrate the equation for u in Eq. (5.8b) and substitute in Eq. (5.8c). By direct integration of Eq. (5.8b) we can write

$$u' = -\frac{\gamma}{2C}|\psi|^2 + a\Delta , \qquad (5.9)$$

where Δ is a dimensionless constant of integration. We choose $\Delta = 0$, which implies that the total length of the polymer is not fixed. Then again, the force constant C can be expressed in terms of the sound velocity S as $C = S^2M/a^2$. Finally, eliminating the displacement u, the system of equation in Eq. (5.8) can be rewritten in the form

$$-2t_0\psi - t_0\psi'' - \chi\psi^3 - g\lambda + \frac{(\omega_X - \mu)\psi}{\sqrt{1 - \psi^2}} = 0 , \qquad (5.10a)$$

$$(\omega_c - \mu)\lambda - \frac{g}{4}\int \psi dv = 0 , \qquad (5.10b)$$

where the coefficient of the cubic term $\chi = D^2/4MS^2$. This system of coupled equation will be solved numerically in Chapter. 6

5.3 Two sites model

In order to check the validity of the BCS trial wave function in Eq. (5.4) and the accuracy of the variational approach, we compare in this section the exact solution of a 2-sites problem with the result obtained with the variational approach. The exact solution is obtained by writing the wave function in the form

$$\Psi = \eta_0|00N_P\rangle + \eta_1|01N_P - 1\rangle + \eta_2|10N_P - 1\rangle + \eta_3|11N_P - 2\rangle ,$$

where the first term in the right-hand side corresponds to the state with zero excitons and N_P photons, the second and third terms describe the states with one exciton and $N_P - 1$ photons, and the last term is a state with two excitons and $N_P - 2$ photons. Here, we assume that the number of polaritons in the system $N_P > 1$. In this section we will also consider the hopping t_{12} as a fixed parameter. Using this form for the wave function in the Schrödinger equation with the Hamiltonian in Eq. (5.1) we obtain a set of equations for η_i:

$$i\dot{\eta}_0 = \omega_c N_P \eta_0 + \frac{g}{2}\sqrt{N_P}(\eta_1 + \eta_2) ,$$
$$i\dot{\eta}_1 = \varepsilon_1\eta_1 + \frac{g}{2}(\sqrt{N_P}\eta_0 + \sqrt{N_P - 1}\eta_3) - t_{12}\eta_2 ,$$
$$i\dot{\eta}_2 = \varepsilon_1\eta_2 + \frac{g}{2}(\sqrt{N_P}\eta_0 + \sqrt{N_P - 1}\eta_3) - t_{12}\eta_1 ,$$
$$i\dot{\eta}_3 = (\omega_c(N_P - 2) + 2\omega_X)\eta_3 + \frac{g}{2}\sqrt{N_P - 1}(\eta_1 + \eta_2) ,$$

where $\varepsilon_1 = \omega_c(N_P - 1) + \omega_X$. The energy spectrum and, in particular, the ground state energy are found by direct diagonalization.

Using the trial wave function approach described in the previous section, we

N_P	E_0, exact	E_0, trial WF
4	2.993	3.089
20	16.928	16.972
100	87.837	87.857
200	177.012	177.027
1000	893.528	893.521

Table 5.1: Ground state energies calculated exactly and using the trial wave functions. The calculations were made using the following set of parameters: $\omega_c = 0.9E_g$, $t_{12} = 0.5E_g$, $g = 0.2E_g$.

find that

$$\langle \alpha, \lambda, \beta, \varphi | H | \alpha, \lambda, \beta, \varphi \rangle = \omega_c \lambda^2 + \omega_X (\beta_1^2 + \beta_2^2) -$$

$$-2t_{12}\alpha_1\beta_1\alpha_2\beta_2 \cos(\varphi_1 - \varphi_2) + g\lambda \sum_{i=1}^{2} \alpha_i \beta_i \cos \varphi_i . \tag{5.11}$$

Without a loss of generality, the following substitutions are made in Eq. (5.11): $\varphi_i = \pi$, $\lambda = \sqrt{N_P - \beta_1^2 - \beta_2^2}$, $\alpha_i = \sqrt{1 - \beta_i^2}$. The resulting expression depends only on β_i. The minimum value of $\langle \alpha, \lambda, \beta, \varphi | H | \alpha, \lambda, \beta, \varphi \rangle$ is considered as the ground state energy. Table 5.1 shows the comparison between the exact and the variational results. The ground state energy was calculated for different values of the photon number in the cavity. The ground state energies calculated with the variational approach are in good agreement with the exact calculation. As expected, the exact ground state energy is slightly smaller than the energy calculated using the trial wave function. This difference can be related to correlation effects not included in the trial wave function. Also notice that the difference between the ground state energy calculated with the two approaches decreases at a larger number of the photons. In fact, the correlation effects between the excitons and the cavity photons are expected to disappear for a photon number much larger that the excitation number in the system.

Chapter 6

Results

In this chapter we will make an analysis of the exciton-lattice interaction in a micro-cavity by solving the system of equations for the polarization function and the cavity field order parameter. The system of Eqs. (5.10) describes the coherent exciton-phonon and exciton-photon interactions, meaning that the phase between the the polarization and the cavity field, which is given in terms of the coherent state, remains constant. This phase is fixed by the dipole exciton-phonon interaction. We keep the cavity field energy below the exciton energy, implying hat we deal with virtual excitons. Thus, dissipation processes are not considered in the system. Also, we assume that the polariton number, which is the total number of photons and excitons, is a conserved quantity for our system. The coupling of polaritons to the lattice brings self-attraction to the system, i.e. exitons appear to be trapped in the self-created matter field. This nonlinear attraction depends both on the exciton density and the deformation potential. Starting from no polaritons and increasing their number, the system goes through several phase transitions due to the change in the excitation regimes.

The system of Eqs. (5.10) is strongly non-linear. It is practically impossible to solve it analytically except for some limiting cases, which we will discuss in Sec. 6.3. Thus, we have to make a numerical analysis. In Sec. 6.1 we describe the

method of functional minimization and how it can be applied to our problem of solving the non-linear system of equations. In the other sections of this Chapter we present analytical results for some limiting cases as well as numerical calculations for the model introduced in Chapter 5. By calculating the chemical potential, we found self-trapping phase transitions, which are also reflected in a sharp change of the exciton/photon number as a function of the polariton number. In Sec. 6.2 we discus the limit of low polariton density when the cubic term in Eq. (5.10a) and correspondingly the self-trapping effect can be neglected. In Sec.6.3 we discuss the self-trapping and analyze the system when the fermionic nature of the excitons can be taking into account as a perturbation. With further increase of the polariton density the internal fermionic structure gives rise to a hard-core repulsive term, leading to the saturation of the exciton state, which we describe in Sec. 6.4. In the last Section we analyze the system in the assumption that the lattice deformation is homogeneous, which allows us to obtain an analytical expression for the total energy by a direct solution of the equation of motion for the excitons and cavity photons.

6.1   Numerical procedure: Steepest descent method of functional minimization

Having established the validity of the variational approach, we can study the general case of a long chain. In order to study on the same ground the inter-cell hopping and the presence of the cavity field we solve the system of Eqs. (5.10) numerically. There are several methods can be used for solving the problem, e.g the Runge-Kutta method, Shooting method, Relaxation method [35]. For the purpose of solving the system, we use the steepest descent method of functional minimization [35]. Several methods have been proposed to improve the method [36]; however, the steepest descent method of functional minimization is efficient enough for
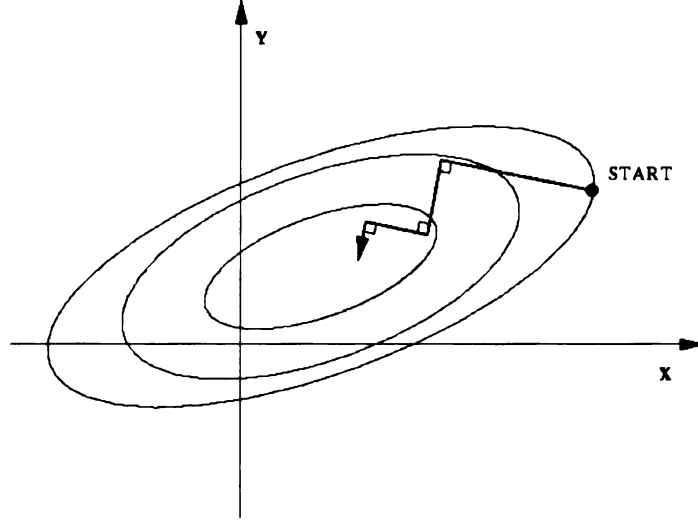
Figure 6.1: T. Hjorteland,*The Action Variational Principle in Cosmology* , Institute of Theoretical Astrophysics University of Oslo (1999). The method of Steepest Descent approaches the minimum in a zig-zag manner, where the new search direction is orthogonal to the previous

solving the system. This method is efficient in solving numerically Gross-Pitaevskii equations for BECs, which are similar to our nonlinear equations [34]. The method consists of projecting an initial trial state onto the minimum of an effective energy $\mathcal{H}$ by propagating the state in an imaginary time. The graphical illustration of the steepest descent method is given in Fig. 6.1. We start from an initial field parameter $\lambda(\tau = 0)$ and a trial function $\psi(\tau = 0)$, then $\lambda(\tau)$ and $\psi(\tau)$ are evaluated in terms of the equations

$$\frac{\partial \psi(\tau)}{\partial \tau} = -\frac{\bar{\delta}\mathcal{H}}{\bar{\delta}\psi_n(\tau)} \tag{6.1}$$

and

$$\frac{\partial \lambda(\tau)}{\partial \tau} = -\frac{\bar{\delta}\mathcal{H}}{\bar{\delta}\lambda(\tau)} , \tag{6.2}$$

where $\bar{\delta}$ indicates a constrained derivative that preserves normalization. Eqs. (6.1) and (6.2) define a trajectory in the parameter space for the optical polarization and the field parameter λ. At each step we move a little bit down the gradient $-\frac{\bar{\delta}\mathcal{H}}{\delta\psi}$ and $-\frac{\bar{\delta}\mathcal{H}}{\delta\lambda}$. The end product of the iteration corresponds to the self-consistent minimiza-

tion of the energy. The time dependence is just a label for different configurations. In practice we chose a step $\triangle\tau$ and iterate the equations

$$\psi(\tau + \triangle\tau) \approx \psi(\tau) - \triangle\tau\frac{\overline{\delta\mathcal{H}}}{\overline{\delta\psi(\tau)}} , \tag{6.3}$$

$$\lambda(\tau + \triangle\tau) \approx \lambda(\tau) - \triangle\tau\frac{\overline{\delta\mathcal{H}}}{\overline{\delta\lambda(\tau)}} \tag{6.4}$$

by normalizing ψ and λ to the total number of polaritons N_P at each iteration. The time step $\triangle\tau$ controls the rate of convergence. The system is described using 100 points and periodic boundary conditions and one parameter for the cavity photon field. As a test we compared our numerical calculations with some analytical limit cases. For the trial initial ψ we used a random values on each site and also a form corresponding to an analytical limit that will be discussed in the next section. The number of iteration depends on the convergence rate and the choice of the initial trial function. Typically, we used $10^5 - 10^6$ iterations.

6.2   Low polariton density

The results of the numerical solution for the function ψ are shown in Fig. 6.2 for the case $\chi = 6t_0$. At very low excitation densities $\rho_P = N_P/N$, where N is the number of sites, polaritons behave as simple bosons. In that limit the self-trapping effect is absent since the nonlinear attractive potential is proportional to the local polariton density and can be neglected in this low density limit. Mathematically, this limit can be described by approximating $\psi/\sqrt{1 - \psi^2} \approx \psi$ in the last term of Eq. (5.10a). The cubic term ψ^3 is not strong enough to give rise to the self-trapping effect in this limit [37]. In other words, a nonhomogeneous solution to Eq. 5.10a would have an overlap much bigger than the periodicity of the system, imposed by the boundary conditions. Note that symmetry-breaking always exists for box boundary conditions, which we do not consider here.
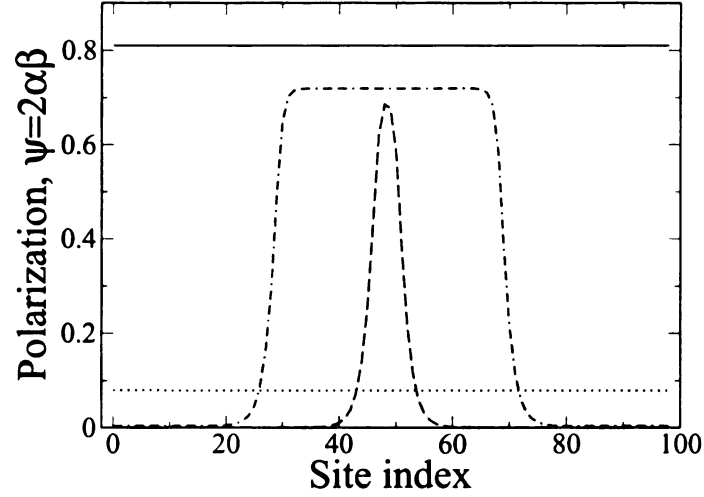
Figure 6.2: Polarization ψ for $\delta/t_0 = 0.01$, $g/t_0 = 0.01$, $\chi/t_0 = 6$, $\rho_P = 3 \times 10^{-3}$ (dotted line), $\rho_P = 6 \times 10^{-3}$ (dashed line), $\rho_P = 6 \times 10^{-2}$ (dot-dashed line), and $\rho_P = 10$ (solid line).

In the absence of the self-attractive term the distribution of the optical polarization is homogeneous. In this low excitation limit the chemical potential μ is simply given by

$$\mu = \frac{1}{2}\left(\omega'_X + \omega_c - \sqrt{\delta^2 + g'^2}\right),$$ (6.5)

where $\omega'_X = \omega_X - 2t_0$ (energy at the bottom of the excitonic band), $\delta = \omega'_X - \omega_c$ is the optical detuning, and $g' = g\sqrt{N}$. Notice that in this limit the chemical potential does not depend on the coefficient of the cubic term in Eq. (5.10). Moreover in this limit the chemical potential corresponds to the energy of the lowest polariton at $k = 0$.

6.3 Intermediate density: self-trapping

By increasing the number of polaritons we observe a critical polariton number at which a polarization symmetry-breaking transition occurs. A similar symmetry-breaking transition was found in the case of BEC with an attractive nonlinear interaction [37]. Our numerical calculations for the dependence of μ on the polariton
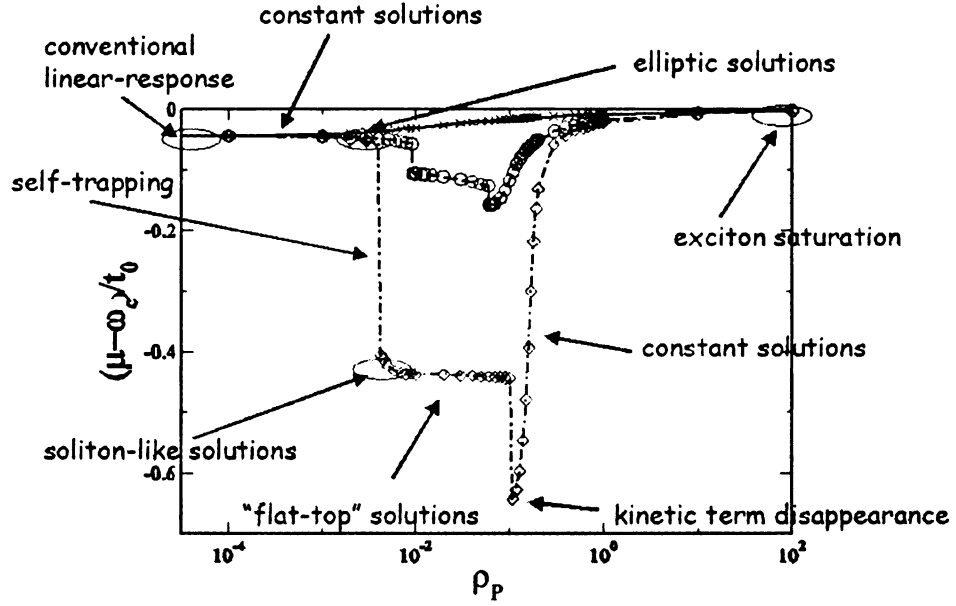
Figure 6.3: Polariton chemical potential as a function of the polariton density for $\delta/t_0 = 0.01$, $g/t_0 = 0.01$, $\chi/t_0 = 0$ (solid line), $\chi/t_0 = 4.5$ (dashed line), and $\chi/t_0 = 6$ (dot-dashed line). Circuses show the analytical solution regions.

density $\rho_P = N_P/N$ are shown in Fig. 6.3 for several values of the cubic term χ, where the circled regions are those we are able to find analytical solutions .

When the exciton number increases following the polariton number, a self-trapping occurs, caused by the polariton-lattice coupling (dashed line in Fig. 6.2). There is a drop in the chemical potential at the point of symmetry-breaking (Fig. 6.3) due to the self-trapping. The breaking of the spatial homogeneity gives a negative contribution to the energy of the system. Also, this makes exciton-like states more energetically favorable than photon-like states, which results in a sharp decrease of the photonic component for nonzero χ, as shown in Fig. 6.4. The self-trapping effect brings a discontinuity both in the chemical potential μ, and in the photon (exciton) density as a function of the polariton density. Since the effective attractive potential depends on both $|\psi|^2$ and χ, the point of symmetry breaking for higher χ corresponds to smaller values of the polariton density $\rho_P = (N_P)/(N)$.

Starting from the small excitation limit, we can expand $\psi/\sqrt{1 - \psi^2} \approx \psi + \frac{1}{2}\psi^3$.
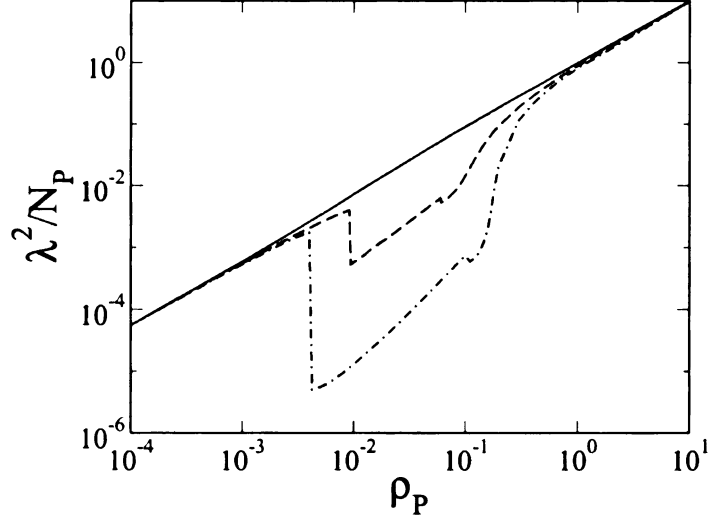
57

Figure 6.4: Photon density as a function of polariton density for $\chi/t_0 = 0$ (solid line), $\chi/t_0 = 4.5$ (dashed line), and $\chi/t_0 = 6$ (dot-dashed line).

The second term introduces an effective repulsion related to the intrinsic fermionic nature of the excitons and decreases the cubic term χ by $(\omega_X - \mu)/2$. In this small excitation limit some analytical forms for the solution to Eq. (5.10a) for the system with a fixed exciton number can be written in terms of Jacobian elliptic functions. Using the identity $\psi'' = \psi'(d\psi'/d\psi)$, we write down Eg. (5.10a) in this limit in the form

$$t_0 \psi' \frac{d\psi'}{d\psi} = -(\chi - \frac{\omega_X - \mu}{2})\psi^3 - g\lambda + (\omega_X - t_0 - \mu)\psi , \tag{6.6}$$

After integrating both the sites of Eq. 6.6, we get

$$t_0 \psi'^2 = -\frac{(\chi - \frac{\omega_X - \mu}{2})}{2}\psi^4 - 2g\lambda\psi + (\omega_X - t_0 - \mu)\psi^2 + d , \tag{6.7}$$

where d is a constant of integration. using the separation of variables and integrating again, we get the expression

$$t_0 \int dv = \int \frac{d\psi}{\sqrt{-(\chi - \frac{\omega_X - \mu}{2})\psi^4/2 - 2g\lambda\psi + (\omega_X - t_0 - \mu)\psi^2 + d}} , \tag{6.8}$$
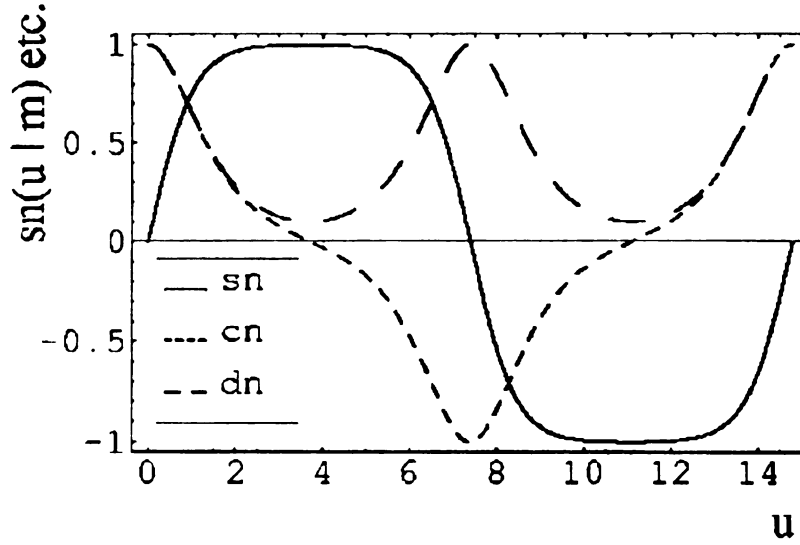
58

Figure 6.5: The three basic Jacobian elliptic functions, for the parameter m=0.99. The solid line is sn, the dotted line is cn, and the dashed line is dn. Note that the period of dn is half that of the other two, and that dn is nodeless. All Jacobian elliptic functions may be constructed from these three. Of the 12 possible functions, these three shapes are the only normalizable ones which differ from each other by more than a translation along the horizontal axis or a renormalization along the vertical axis [37].

which is an elliptic integral. It is always possible to express an elliptic integral as a sum of normal elliptic integrals of the first, second, and the third kinds [38]. Then by the use of Cayley transformation [39] Eq. (6.8) can be inverted, and $\psi(v)$, which is the solution to the polarization function, can be given in terms of the Jacobian elliptic functions. There is a total of 12 such functions. Only three of them (sn, cn and dn) have distinct physical forms. The function $sn(u|m)$ may be written in the integral form,

$$u = \int_0^x \frac{dt}{\sqrt{1 - t^2}\sqrt{1 - mt^2}},$$ (6.9)

where $u = sn^{-1}(x)$ so that $x = sn(u|m)$. The functions $cn(u|m)$ and $dn(u|m)$ may then be defined by the equations

$$cn(u|m) = \sqrt{1 - sn^2(u|m)},$$
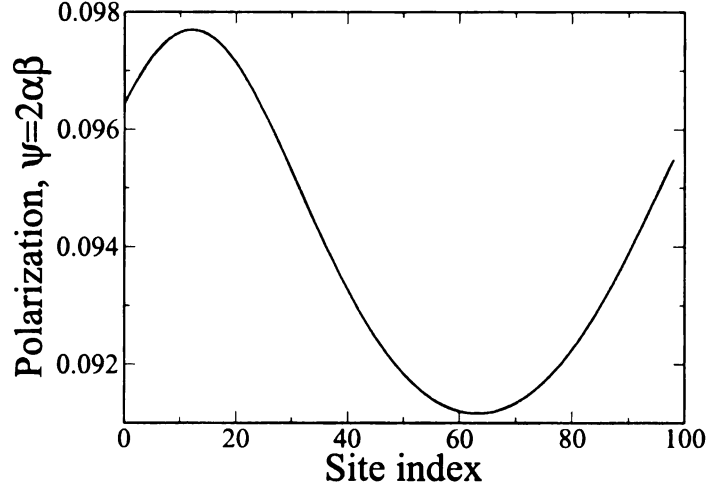$$dn(u|m) = \sqrt{1 - msn^2(u|m)}.$$ (6.10)

Figure 6.6: Polarization ψ for $\delta/t_0 = 0.01$, $g/t_0 = 0.01$, $\chi/t_0 = 6$, $\rho_P = 4 \times 10^{-3}$ near the symmetry-breaking point.

We plot them in Fig. 6.5. The limits of the sn, cn and dn, along with complete elliptic integrals $K(m)$ and $E(m)$, are listed in Table 6.1. The period of the sn and cn functions is $4K(m)$, while that of the dn function is $2K(m)$.

Particularly, if we neglect the second term in the right hand side of Eq. (6.7), the solution to the nonlinear Schrödinger equation (NLSE) is given by one of the Jacobian elliptic functions. The cn function solves the NLSE for repulsive nonlinearity, while only the cn and dn functions solve the NLSE for attractive nonlinearity. Only the dn function satisfies the periodic boundary conditions in the assumption that the polarization function does not vanish ($\psi_n > 0$). Thus, it should be a solution for the optical polarization to the nonlinear equation (5.10a) when the excitonic number is greater the photon one. If the cubic term of the NLSE is weak, the para-

	m=0	m=1
$sn(u\vert m)$	$\sin(u)$	$\tanh(u)$
$cn(u\vert m)$	$\cos(u)$	$sech(u)$
$dn(u\vert m)$	1	$sech(u)$
$K(m)$	$\pi/2$	∞
$E(m)$	$\pi/2$	1

Table 6.1: Limits of Jacobian Elliptic functions and integrals [40]

60

meter $m \to 0^+$ and dn $\to 1$. In the opposite case of the strong nonlinear attraction, $m \to 1^-$ and dn $\to$ sech, that leads to the function collapse in a sharp peak. The numerical solution for the polarization ψ near the symmetry breaking is shown in Fig. 6.6. The shape of the function plot corresponds to dn, which looks like an asymmetric wave function on top of the constant solution. This solution is unstable and has a very slow convergence.

With a small increase of the polariton number ρ_X the excitonic component starts to significantly exceed the photonic one because the self-trapping makes it energetically favorable. The polarization function collapses in a sharp peak because of the strong nonlinear attraction. In case when the photon number is much smaller than the exciton number, we can neglect the fourth term in Eq. (5.10a), since as seen from Eq. (5.10b), λ is inversely proportional to $\omega_c - \mu$. In this limit, when the localization length is much smaller than that of the chain, the solution can be written in the form

$$\psi = A\mathrm{sech}[Y(\nu - \nu_0)] , \tag{6.11}$$

where

$$Y = \frac{(\chi - \frac{\omega_X - \mu}{2})N_P}{4t_0} , \tag{6.12}$$

$$A = \sqrt{\frac{YN_P}{2}} , \tag{6.13}$$

and the chemical potential is determined by the equation

$$\mu = \omega_X - 2t_0 - \frac{(\chi - \frac{\omega_X - \mu}{2})^2 N_P^2}{16t_0} . \tag{6.14}$$

Alternatively, we can say that when the cubic term in the Eq. (5.10a) is quite strong $m \to 1$ and $\mathrm{dn}(u|m) \to \mathrm{sech}(u)$
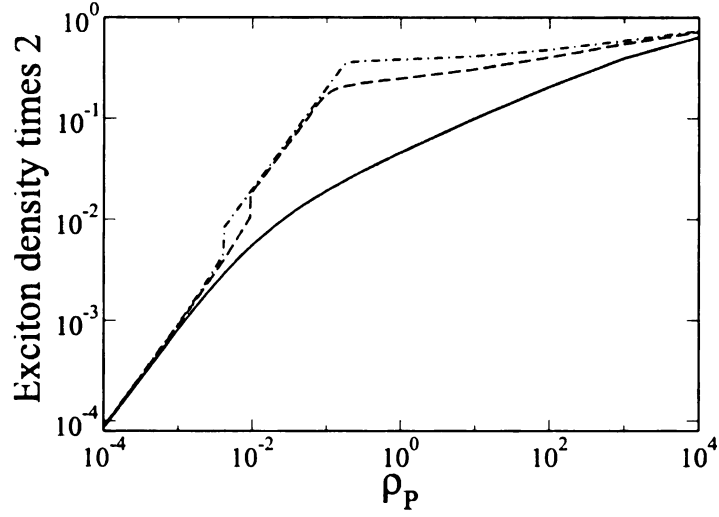
Figure 6.7: Exciton density times 2 as a function of the polariton density for $\chi/t_0 = 0$ (solid line), $\chi/t_0 = 4.5$ (dashed line), and $\chi/t_0 = 6$ (dot-dashed line).

6.4 Saturation

By further increasing the polariton density, the internal fermionic structure of the excitons gives rise to a hard-core repulsion term, which leads to the saturation of the exciton states, making the polarization distribution broader and flatter at the top (dot-dashed line in Fig. 6.2). When the saturation spreads over the whole chain length, the polarization distribution (solid line in Fig. 6.2) becomes homogeneous again. We expect a discontinuity of μ again at this point as a consequence of the disappearance of the gradient of the polarization function (kinetic term), which gives a positive contribution to the energy. With the further increase of the exciton density the hopping effect is reduced due to the blocking. Fig. 6.7 shows the exciton density $\int |\beta|^2 dv / N$ multiplied by 2 as a function of ρ_P, which reaches 1 in the limit of large excitation density regardless the value of χ, corresponding to half filling of the exciton band. The half filling maximizes the polarization and hence minimizes the dipole interaction energy between the excitons and the cavity photons. In this saturation regime the polaritons become photon-like, since an added excitation mainly contributes to the cavity mode, and thus the chemical potential
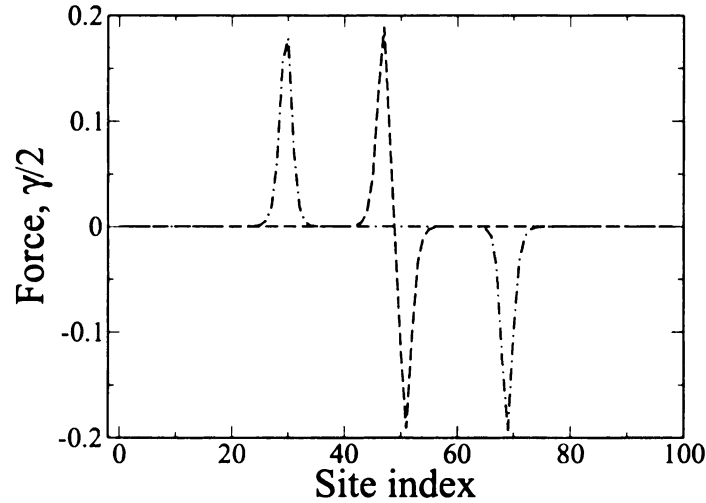
Figure 6.8: Force as a function of the site index for $\chi/t_0 = 6$, $\rho_{ex} = 6 \times 10^{-3}$ (dashed line), $\rho_{ex} = 6 \times 10^{-2}$ (dot-dashed line).

finally approaches ω_c (see also Fig. 6.3). In this saturation regime the expressions for the polarization function ψ and the chemical potential μ are given by the following expressions

$$\psi = \frac{\Omega}{\sqrt{\delta^2 + \Omega^2}} \tag{6.15}$$

and

$$\mu = \omega_c - \frac{g'^2}{4\sqrt{\delta^2 + \Omega^2}}, \tag{6.16}$$

where $\Omega = g\sqrt{N_P}$, $g' = g\sqrt{N}$, and $\delta = \omega_\chi - \omega_c$.

A gradient in the density of polarization produces a force on the ions according to Eq. (5.8b). The force is stronger at the edges of the saturation region of the $|\psi|^2$ distribution as seen in Fig. 6.8, and is positive to the left from the center of the symmetry-breaking point and negative to the right. This reduces of the total length of the chain due to the interaction with the electromagnetic cavity mode.

The classical displacements due to such a force, which can be found from Eqn. 2.29, with the corresponding scheme of the chain distortions, are shown in Fig. 6.9 for $\delta/t_0 = 0.01$, $g/t_0 = 0.01$, $\chi/t_0 = 6$, $\rho_P = 6 \times 10^{-2}$. It shows a significant change in the region of the exciton localization.
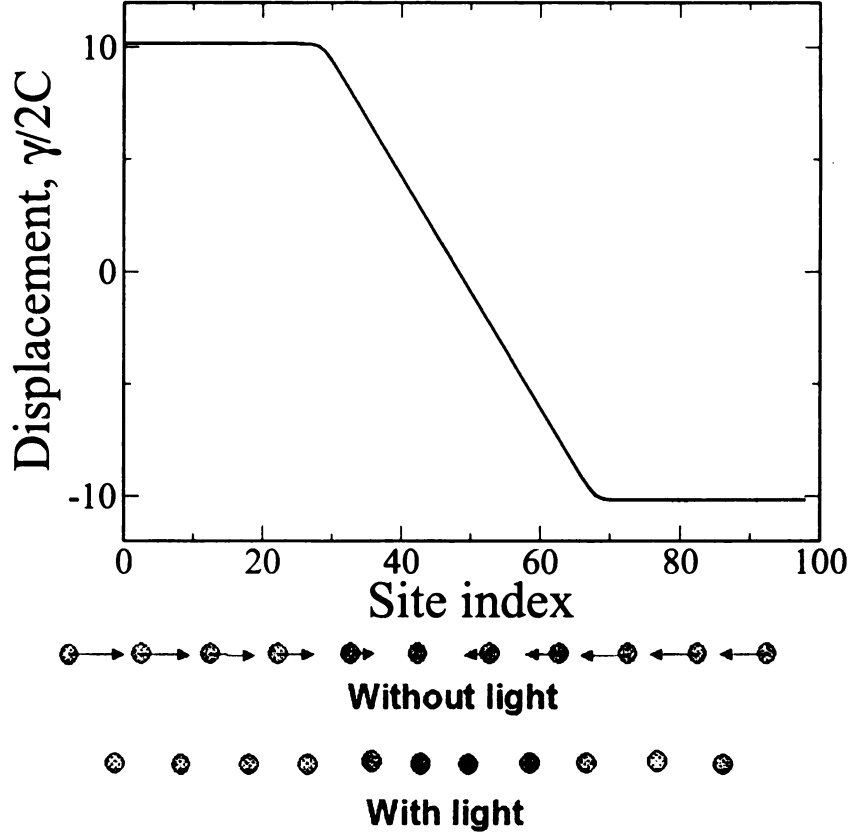
63

Figure 6.9: Displacement due to the force as a function of the site index for $\delta/t_0 = 0.01$, $g/t_0 = 0.01$, $\chi/t_0 = 6$, $\rho_P = 6 \times 10^{-2}$ and the corresponding scheme of the chain distortions showing the position of atoms before and after the system excitation.

6.5 Homogeneous deformation and role of damping

The lattice deformation in the presence of optical excitations can be understood by analyzing the total energy of the system in the assumption that the lattice deformation is homogeneous [41], [42]. As seen in the previous section, this assumption is justified for a systems in the saturation regime or for a polariton density below the critical value for self-trapping. The total energy of the lattice is modified by the presence of polaritons. The homogeneous deformation allows us to obtain an analytical expression for the total energy of the system, and to analyze the effect of the finite linewidth of polaritons. We will include both the spontaneous emission

64
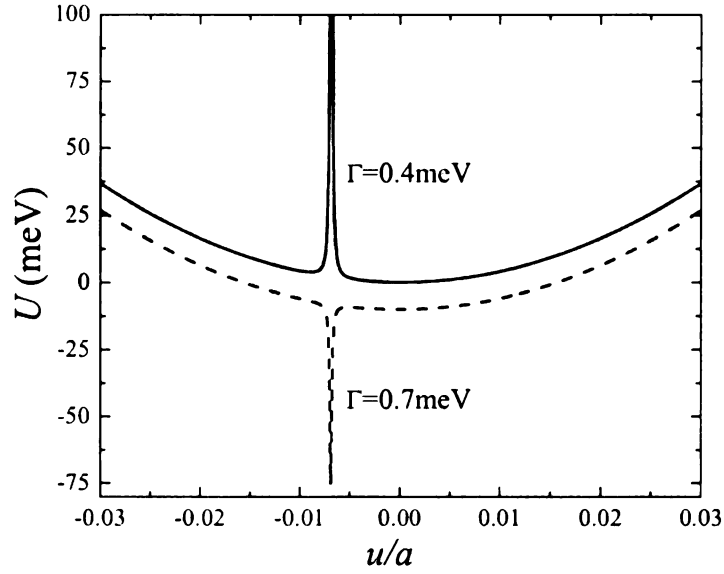
Figure 6.10: Effective lattice potential as a function of displacement. The figure has been obtained for the following set of parameters: $E_g = \omega_X - 2t_0 = 2.282$ eV, $D = 2\gamma a = 6.1$ eV, $S = 2.5 \cdot 10^3$m/s, $a = 1.5$ nm, $M = 2.110^{-21}$ g, $\omega_0 = 2.282$ eV, and $C = S^2 M/a^2 = 82eV/a^2$. The excitation corresponds to $\rho_{ex} \sim 0.1$. $\alpha_c = g' = 1$ meV, and $\omega_c = 2.242$ eV. $\Gamma = 400$ μeV and $\Gamma = 700$ μeV for the upper and lower curve, respectively. The curves are displaced for clarity.

of the excitons and the finite Q factor of the cavity mode. Instead of using the variational approach of Chapter 5, we will solve directly the equations of motion for the excitons and cavity photons.

We start by using the Fourier transform

$$B_n = \frac{1}{\sqrt{N}} \sum_k e^{ikna} b_k \, , \tag{6.17}$$

where N is the number of lattice sites, k is the wave vector, and a is the lattice separation, to define the operator b_k as the annihilation operator of an exciton with a wave vector k. The Hamiltonian in Eq. (5.1) can then be rewritten as

$$
\begin{aligned}
H = \sum_n &\left[\frac{p_n^2}{2M} + \frac{C}{2} (u_{n+1} - u_n)^2 \right] + \\
&+ \sum_k \omega_k b_k^\dagger b_k + \sum_{k,k'} f(k,k') b_k^\dagger b_{k'} \\
&+ \omega_c c^\dagger c + \frac{g'}{2} c^\dagger b_0 + \frac{g'}{2} c b_0^\dagger \, ,
\end{aligned}
\tag{6.18}
$$

where $\omega_k = \omega_X - 2t_0 \cos(ka)$ and

$$
\begin{aligned}
f(k,k') = \frac{\gamma}{N} \sum_n &(u_{n+1} - u_n) \times \\
&\times \left[e^{-ika} e^{ina(k-k')} + e^{ik'a} e^{ina(k'-k)} \right] .
\end{aligned}
\tag{6.19}
$$

We consider a finite-length chain with periodic boundary conditions. The equilibrium lattice displacement is homogeneous and will be indicated by $u = u_{n+1} - u_n$. Notice that in this limit $f(k,k')$ is diagonal

$$f(k,k') = 2\gamma \cos(ka) u \delta_{k,k'} \, . \tag{6.20}$$

Eqs. (6.20) and (6.18) show that in this homogeneous case there is no mixing of polariton with different k vector. Since the cavity couples to the $k = 0$ exciton

mode only, the polariton modes at $k \neq 0$ are completely decoupled and do not enter in the dynamics. Taking into account Eq. (6.20), the excitonic part in H reduces to $\omega_0(u)b_0^\dagger b_0$, where $\omega_0(u) = \omega_X - 2t_0 + 2\gamma u$ is the energy of the exciton at $k = 0$ renormalized by the lattice deformation potential. We also add a term that describes the pumping of the cavity mode by an external field and represent the full system by

$$H = \sum_n \left[\frac{p_n^2}{2M} + \frac{Cu^2}{2} \right] +$$
$$+\omega_0(u)b_0^\dagger b_0 + \frac{g'}{2}(c^\dagger b_0 + b_0^\dagger c) + \omega_c c^\dagger c +$$
$$\frac{\kappa E_0}{2}(c e^{i\omega ct} + c^\dagger e^{-i\omega ct}) , \qquad (6.21)$$

where E_0 represents the electric field of the external pump and κ is the coupling between the external pump and the cavity mode. The operators B_n are fermionic on the same site, but commute for different sites. Therefore, the commutation relation for b_0 reads

$$[b_0, b_0^\dagger] = 1 - \frac{2\sum_n B_n^\dagger B_n}{N} . \qquad (6.22)$$

Since we will assume here that there are no excitations of phonon modes at $k \neq 0$, we have that $\sum_N B_n^\dagger B_n = \sum_k b_k^\dagger b_k \sim b_0^\dagger b_0$. The equations for the expectation values of the polarization $\langle b_0 \rangle = p$, exciton density $\langle b_0^\dagger b_0 \rangle = n_X$ and cavity photon operator $\langle c \rangle = \lambda$ can be obtained using the standard factorization scheme [43] and read

$$\dot{\lambda} = -i \left[\omega_c \lambda + \frac{g'}{2}p + \frac{\kappa E_0}{2}e^{-i\omega ct} \right] - \alpha_c \lambda , \qquad (6.23)$$

$$\dot{p} = -i \left[\omega_0(1 - \frac{2n_X}{N})p + \frac{g'}{2}\lambda(1 - \frac{2n_X}{N}) \right] - \Gamma p , \qquad (6.24)$$

$$\dot{n}_X = -i\frac{g'}{2}(1 - \frac{2n_X}{N})(p^*\lambda - p\lambda^*) - 2\Gamma n , \qquad (6.25)$$

where we have introduced the spontaneous emission rate of the excitons Γ and

the damping of the cavity mode α_c, due to the finite Q-factor of the cavity. The equation for λ can be explicitly integrated and gives

$$i\lambda = \frac{g'}{2}\frac{p}{\alpha_c} + \frac{\kappa E_0}{2\alpha_c}e^{-i\omega_c t} . \tag{6.26}$$

This expression can be used in Eqs. (6.24) and (6.25) which give for the steady state

$$\tilde{p} = \left(-i\frac{g'}{2}\frac{\kappa E_0}{2\alpha_c}(1 - \frac{2n_X}{N})\right) \bigg/ \left(\omega_c - \omega_0(1 - \frac{2n_X}{N}) + i\Gamma + i\frac{g'^2}{4\alpha_c}(1 - \frac{2n_X}{N})\right) , \tag{6.27}$$

where we have defined $p = \tilde{p}e^{-i\omega_c t}$.

The u-dependent total potential energy $U(u)$ of the system can be obtained by substituting the solution for p, λ, and n_X which depend on u, into the initial Hamiltonian(6.21). At weak excitation we obtain

$$U(u) \sim \frac{NC}{2}u^2 + \omega_0(u)n_X(u) +$$

$$+\omega_c\left[\left(\frac{g'}{2\alpha}\right)^2 - \frac{2\Gamma}{\alpha_c}\right]n_X(u) + \omega_c I \tag{6.28}$$

where $I = (\kappa E_0/2\alpha_c)^2$ and

$$n_X(u) \sim |p|^2 = \frac{I(g'/2)^2}{(\delta + 2\gamma u)^2 + \Gamma^2} . \tag{6.29}$$

Notice that n_X has a resonant behavior as a function of u, which is a consequence of the deformation potential shift in the excitonic energy.

In the absence of light the potential energy U depends quadratically on u with a minimum at $u = 0$. When the laser is switched on, this dependence changes due to the presence of optical excitations in the system. Due to the resonant behavior in Eq. (6.29), it is energetically favorable to have $u \neq 0$ if this reduces the total energy of the system. Figure 6.10 shows the potential energy for some values of parameters. The parameters used in these calculations are typical of polydiacety-

68

lene chains. We observe that the potential U has a parabolic dependence with a superposed Lorentian contribution due to the optical excitation. This Lorentian contribution can be either positive or negative depending on the relative strength of the exciton-cavity coupling, spontaneous emission rate and cavity damping. The actual behavior can be explicitly calculated using Eq. (6.28). In the figure we consider two particular sets of parameters providing a minimum of the energy that corresponds to contraction and expansion of the lattice.

Conclusions

The main part of this thesis has been devoted to the analysis of the exciton-photon system interacting with the lattice. We have investigated the optically-induced lattice strain in a single polymer chain in a cavity. We have extended the excitonic SSH model, describing the exciton propagation in the chain, to include the effect of the cavity electromagnetic field. Using a polariton picture, we have obtained a system of integro-differential nonlinear equations for the spatial distribution of the optical excitations in the chain. At low excitation regime we have been able to get analytical solutions to this system of equations in terms of the Jacobian elliptic functions. Numerical calculations have been performed by the use of the steepest descent method of functional minimization. We find solutions describing a self-trapping of the polaritons which saturate when the excitation density is increased. This saturation induced by the hard-core repulsion is related to the internal fermionic structure of excitons.

The chemical potential of the polaritons shows a discontinuity at a threshold value of the polariton density. This critical density corresponds to the onset of the self-trapping. The self-trapping causes a sharp increase in the excitonic component and decrease in the photonic component of the polariton wave function. With the polariton density increase the system becomes more photon-like because of the excitonic part saturation. That makes the chemical potential approach the cavity photon energy in the limit of the high excitation.

We have also considered the role of the finite radiative recombination rate of the

excitons and the finite Q factor of the cavity. These can be studied in a direct way in the case of a homogeneous strain field. We have found that both a contraction and expansion of the lattice are possible, depending of the relative strength of the exciton-cavity coupling, radiative recombination, and cavity Q factor.

We have neglected exciton-exciton Coulomb effects, which may affect the picture, especially in the high excitation regime. This deserves further investigations. However, it is known that the BCS variational ansatz in Eq. (5.4) provides a good description of the ground state of an electron-hole system both in the low excitation regime (excitonic BEC) and in the high excitation regime (BCS pairing) [44]. The fact that the electron-hole system here interact with the cavity electromagnetic field gives an additional justification to this ansatz since light-dressing can reduce Coulomb features beyond mean field like screening and broadening [45]. The exciton-exciton correlations may change the magnitude of the effective parameters such as the electrom/hole dispersion and the coupling constant [46].

The results suggest that local lattice deformations can be finely controlled by the polariton density and detuning. This control scheme could have interesting applications not only to polymers but also to some other organic materials where a strong exciton-phonon interaction exists, like e.g. in J-aggregates, or DNA [47]. Recently-developed experimental techniques can detect light-induced lattice displacement in molecules and semiconductor systems. The quantity that is measured in electron or x-ray diffraction experiments would be $\partial u_n / \partial n$, i.e. the local deformation due to the light-induced changes in the lattice. Typically this quantity is in the range $10 - 100$ $m\text{Å}$, which is reasonable for an experimental observation of the effect. As an example, we can propose to use ultrafast electron diffraction (UED) to detect light-induced lattice displacement [48]. A typical second-generation UED apparatus is composed of a pulse laser, a picosecond electron gun, a free-jet expansion source, and a singe-electron detection system. Diffraction images are recorded with and without the system excitation by a charge-coupled device camera at the

end of a phosphor scintillator-fiber optic-image intensifier chain in the detector chamber. This technique has a spatial resolution of about a milliangstrom. In these experiments the laser pulse is typically used to thermally excite a system. The electron diffraction is then used for the detection of structural changes due to heating. The structural changes discussed in this thesis have a completely different nature, since they originate from the strong exciton-light and exciton-lattice coupling. In contrast to heating, the coherent nature of the exciting field is important in the structural deformations we have investigated. The results of this thesis could open to novel investigations on this *coherent melting*, based on laser and optical control in condensed matter systems.

Bibliography

[1] J. G. Müller, U. Lemmer, G. Raschke, M. Anni, U. Scherf, J. M. Lupton, and J. Feldmann, *Linewidth-Limited Energy Transfer in Single Conjugated Polymer Molecules*, Phys. Rev. Lett. **91**, 267403 (2003)

[2] T. Guillet, J. Berréar, R. Grousson, J. Kovensky, C. Lapersonne-Meyer, M. Shott, and V. Voliotis, *Emission of a Single Conjugated Polymer Chain Isolated in Its Single Crystal Monomer Matrix*, Phys. Rev. Lett. **87** 087401 (2001).

[3] F. Dubin, J. Berréar, R. Grousson, T. Guillet, C. Lapersonne-Meyer, M. Shott, and V. Voliotis, *Optical evidence of a purely one-dimensional exciton density of states in a single conjugated polymer chain*, Phys. Rev. B **66** 113202 (2002).

[4] F. Dubin, R. Melet, T. Barisien, R. Grousson, L. Legrand, M. Shott, and V. Voliotis, *Macroscopic coherence of a single exciton state in an organic quantum wire*, Nature Physics **2** 32 (2006).

[5] R. H. Dicke, *Coherence in Spontaneous Radiation Processes*, Phys. Rev. **93**, 99 (1954).

[6] W. P. Su, J. R. Schrieffer and A. J. Heeger, *Soliton excitations in polyacetylene*, Phys. Rev. B, **22** 2099 (1980).

[7] E. G. Wilson, *A new theory of acoustic solitary-wave polaron motion, Polarons and exciton-polarons in one dimension: the case of polydiacetylene*, J. Phys. C **16** 6739 (1983); *ibidem* **16** 1039 (1983).

[8] A. J. Heeger, S. Kivelson, J. R. Schrieffer and W. P. Su, *Solitons in conducting polymers*, Rev. Mod. Phys. **60**, 781 (1988).

[9] M. H. Szymanska and P. B. Littlewood, *The crossover between lasing and polariton condensation in optical microcavities*, Solid State Commun. **124**, 103 (2002).

[10] Y. Toyozawa, *Optical Processes in Solids*, Cambridge University Press, Cambridge (2003).

[11] H. Deng, G. Weihs, C. Santori, J. Bloch, and Y. Yamamoto, *Condensation of Semiconductor Microcavity Exciton Polaritons*, Science **298** 199 (2002).

[12] H. Deng, G. Weihs, D. Snoke, J. Bloch, and Y. Yamamoto, *Polariton Lasing Vs. Photon Lasing in a Semiconductor Microcavity*, Proc. Nat. Acad. Sci. **100** 15318 (2003).

[13] M. Saba *et al.*, *High-temperature ultrafast polariton parametric amplification in semiconductor microcavities*, Nature **414**, 731 (2001).

[14] B. I. Greene, J. Orenstein, and S. Schmitt-Rink, *All-optical nonlinearities in organics*, Science **247** 679 (1990); B. I. Greene *et al.*, *Phonon-Mediated Optical Nonlinearity in Polydiacetylen*,Phys. Rev. Lett. **61** 325 (1988).

[15] F. Dubin, J. Berréar, R. Grousson, M. Shott, and V. Voliotis, *Evidence of polariton-induced transparency in a single organic quantum wire*, Phys. Rev. B **73** 121302(R) (2006).

[16] K. S. Song and R. T. Williams, *Self-trapped excitons*, Springer, Berlin (1996).

[17] *Polydiacetylenes*, edited by D. Bloor and R. R. Chance, NATO Advanced Study Institute, Series B: Physics (Nijhoff, Dordrecht, 1985).

[18] *Polydiacetylenes*, edited by D. Bloor and R. R. Chance, NATO Advanced Study Institute, Series B: Physics (Nijhoff, Dordrecht, 1985).

[19] V. M. Agranovich, M. Litinskaia, and D. G. Lidzey, *Cavity polaritons in microcavities containing disordered organic semiconductors*, Phys. Rev. B **67**, 085311 (2003).

[20] Y. Toyozawa, *Self-Trapping of an Electron by the Acoustical Mode of Lattice Vibration*, Prog. Theor Phys. **26** 29 (1961).

[21] A. J. Heeger, S. Kivelson, J. R. Schrieffer and W. P. Su, *Solitons in conducting polymers*, Rev. Mod. Phys. **60**, 781 (1988).

[22] H. Zoubi and G. C. La Rocca, Phys. Rev. B **72**, *Exciton-polariton kinematic interactions in organic microcavities*, 125306 (2005)

[23] S. A. Moskalenko and D.W. Snoke,*Bose-Einstein Condensation of Excitons and Biexcitons* (Cambridge University Press, Cambridge, 2000).

[24] E. Hanamura and H. Haug, *Condensation effects of excitons*, Phys. Rep. **33**, 209 (1977).

[25] J. Bardeen and W. Shochley, *Deformation Potentials and Mobilities in Non-Polar Crystals*, Phys. Rev. **80**, 72 (1950).

[26] G. Whitfield and P. B. Shaw, *Interaction of electrons with acoustic phonons via the deformation potential in one dimension*, Phys. Rev. B **14**,3346(1976).

[27] www.pwscf.org

[28] P. Hohenberg and W. Kohn, *Inhomogeneous Electron Gas*, Phys. Rev. **136**, B864 (1964).

[29] W. Kohn, L. J. Sham, *Self-Consistent Equations Including Exchange and Correlation Effects*, Phys. Rev. **140**, A1133 (1965).

[30] P. Giannozi, G. Grosso and G. Pastory Parravichi, *Theory of Electron States in Lattice and Superlattices*, Rivista Del Nuova Cimento26 N.3 (1990).

[31] P. Meystre, M. Sargent III, *Elements of Quantum Optics*, Berlin; New York: Springer-Verlag (1990).

[32] P. R. Eastham and P. B. Littlewood, *Bose condensation of cavity polaritons beyond the linear regime:The thermal equilibrium of a model microcavity*, Phys. Rev. B **64** 235101 (2001).

[33] R.J. Glauber, *Coherent and Incoherent States of the Radiation Field*, Phys. Rev. **131** 2766 (1963).

[34] F. Dalfovo and S. Stringari, *Bosons in anisotropic traps: Ground state and vortices*, Phys. Rev. A **53**, 2477 (1996).

[35] W.H. Press, Saul A. Teukolsky, W.T. Vetterling, B.P. Flannery *Numerical Recipes in Fortran 77*, Cambrige University.

[36] I. Štich, R. Car, M. Parrinello, and S. Baroni, *Conjugate gradient minimization of the energy functional: A new method for electronic structure calculation*, Phys. Rev. B **39** 4997 (1989).

[37] L. D. Carr, C. W. Clark, and W. P. Reinhardt, *Stationary solutions of the one-dimensional nonlinear Schrödinger equation. I. Case of repulsive nonlinearity, Stationary solutions of the one-dimensional nonlinear Schrödinger equation. II. Case of attractive nonlinearity* Phys. Rev. A **62**, 063611 (2000); *ibidem* **62**,063610(2000).

[38] *Nandbook of Elliptic Integrals for Engineers and Scientists*, Springer-Velag, New York, Heidenberg, Berlin, (1971).

[39] *Introduction to elliptic functions*, John Wiley and Songs, Inc, New York (1953).

[40] *Handbook of Mathematical Functions*, edited by M. Abramowitz and I.A. Stegun, National Bureau of Standards, Washington, DC (1964).

[41] M. V. Katkov, Y. V. Pershin, and C. Piermarocchi, *Theory of cavity-polariton self-trapping and optical strain in polymer chains*, Phys. Rev. B **74**, 1 (2006)

[42] Part of the results in this we obtained in cooperation with Dr.Y. Pershin.

[43] V. M. Axt and A. Stahl, *A dynamics-controlled truncation scheme for the hierarchy of density matrices in semiconductor optics*, Z. Phys. B **93**, 195 (1994).

[44] C. Comte and P. Nozières, *Exciton bose condensation - the ground-state of an electron-hole gas .1. Mean field description of a simplest model*, J. Physique **43** 1069 (1982).

[45] C. Ciuti *et al.*, *Strongly Driven Exciton Resonances in Quantum Wells: Light-Induced Dressing versus Coulomb Scattering*, Phys. Rev. Lett. **84**, 1752 (2000).

[46] I. E.Perakis and T.V. Shahbazyan, *Canonical transformation approach to the ultrafast nonlinear optical dynamics of semiconductors*, Int.J. Mid. Phys. B **13**, 869 (1999).

[47] E. M. Conwell and S. V. Rakhmanova, *Polarons in DNA*, Proc. Natl. Acad. Sci. USA **97** 4556 (2000).

[48] H. Ihee *et al.*, *Direct Imaging of Transient Molecular Structures with Ultrafast Diffraction*, Science **291** 458 (2001).